[American Journal of Science, Vol. 316, October, 2016, P. 778–812, DOI 10.2475/08.2016.03]

SUBSIDENCE CONTROL ON RIVER MORPHOLOGY AND GRAIN SIZE IN THE GANGA PLAIN

ELIZABETH H. DINGLE*,†, HUGH D. SINCLAIR*, MIKAËL ATTAL*, DAVID T. MILODOWSKI**, and VIMAL SINGH***

ABSTRACT. The Ganga Plain represents a large proportion of the current foreland basin to the Himalaya. The Himalayan-sourced waters irrigate the Plain via major river networks that support approximately 10 percent of the global population. However, some of these rivers are also the source of devastating floods. The tendency for some of these rivers to flood is directly linked to their large scale morphology. In general, the rivers that drain the east Ganga Plain have channels that are perched at a higher elevation relative to their floodplain, leading to more frequent channel avulsion and flooding. In contrast, those further west have channels that are incised into the floodplain and are historically less prone to flooding. Understanding the controls on these contrasting river forms is fundamental to determining the sensitivity of these systems to projected climate change and the growing water resource demands across the Plain. Here, we present a new basin scale approach to quantifying floodplain and channel topography that identifies areas where channels are super-elevated or entrenched relative to their adjacent floodplain. We explore the probable controls on these observations through an analysis of basin subsidence rates, sediment grain size data and sediment supply from the main river systems that traverse the Plain (Yamuna, Ganga, Karnali, Gandak and Kosi rivers). Subsidence rates are approximated by combining basement profiles derived from seismic data with known convergence velocities; results suggest a more slowly subsiding basin in the west than the east. Grain size fining rates are also used as a proxy for relative subsidence rates along the strike of the basin; the results also indicate higher fining rates (and hence subsidence rates for given sediment supply) in the east. By integrating these observations, we propose that higher subsidence rates are responsible for a deeper basin in the east with perched, low gradient river systems that are relatively insensitive to climatically driven changes in base-level. In contrast, the lower subsidence rates in the west are associated with a higher elevation basin topography, and entrenched river systems recording climatically induced lowering of river base-levels during the Holocene.

Keywords: Subsidence, grain size, Ganga Plain, river morphology, topographic analysis

INTRODUCTION

Many of the rivers of the Ganga Plain are prone to abrupt switching of channel courses (avulsion) causing devastating floods over some of the most densely populated regions on the globe. The Kosi River that drains central Nepal and discharges onto the Ganga Plain of Bihar State has a well-documented history of frequent channel avulsion and flooding (Wells and Dorr, 1987). During 2008, a single channel avulsion event resulted in a temporary eastward shift of the Kosi River by tens of kilometers where the channel breached its eastern levee resulting in extensive flooding (Sinha and others, 2005, 2013, 2014a; Chakraborty and others, 2010). Similarly, levee failures and channel avulsion resulted in catastrophic flooding of the Indus Plain of Pakistan in 2010 and the displacement of at least 10 million people (Syvitski and Brakenridge, 2013). The

* School of GeoSciences, University of Edinburgh, Drummond Street, Edinburgh, EH10 5EQ, United Kingdom
** School of GeoSciences, University of Edinburgh, Crew Building, Edinburgh, EH9 3JN, United Kingdom
*** Department of Geology, University of Delhi, Delhi 110007, India
† Corresponding author: elizabeth.dingle@ed.ac.uk

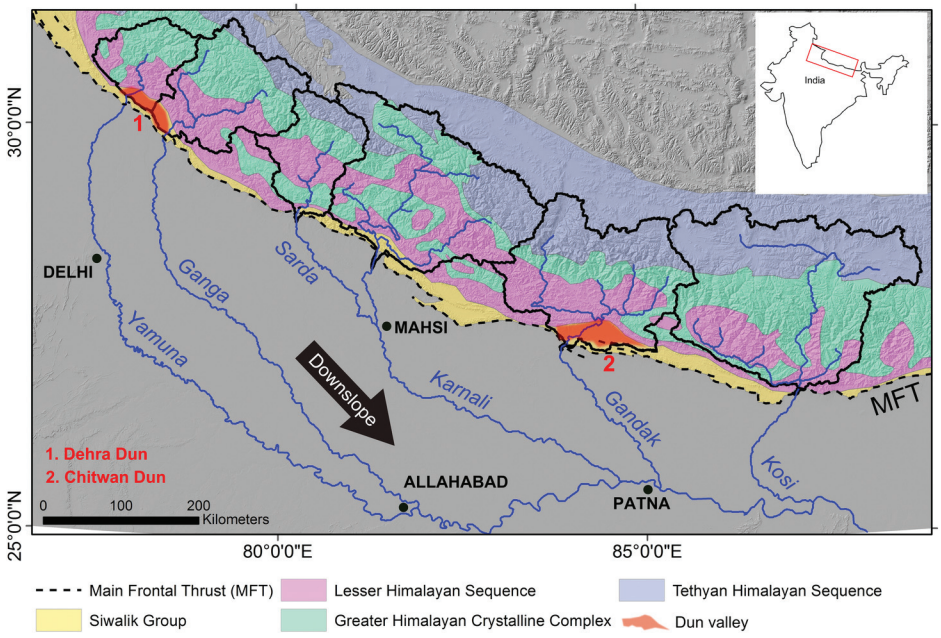

Fig. 1. Study catchments, location of major Dun valleys and geology (from Yin, 2006) in the Ganga basin on a 90 m Shuttle Radar Topography Mission (SRTM) derived Digital Elevation Model (DEM).

nature and frequency of channel avulsion is also a first-order control on alluvial stratigraphy, defining the geometric distributions of channel and floodplain deposits (Bridge and Leeder, 1979; Slingerland and Smith, 2004). In the Ganga Plain, the distribution of Quaternary channel sands and floodplain muds determines groundwater pathways and associated arsenic pollution (Shah, 2007). Given the significance of floodwaters and groundwater pathways in the Ganga Plain, documenting and understanding variations in the morphology of river channel and floodplain systems represents a research priority, particularly in light of changes in monsoon intensity, glacial meltwater discharge and the water demands of a growing population (Fleitmann and others, 2007; Immerzeel and others, 2010).

Systematic variations in the large-scale morphology of the river systems are recognized across the extent of the Ganga foreland basin (fig. 1) (Sinha and others, 2005). Rivers of the east Ganga Plain are characterized by shallow aggrading channels that frequently avulse and flood, whilst those in the west are characterized by degrading systems with incised channels and extensive areas of badland topography. In the east Ganga Plain, numerous channel avulsions and random switching of the loci of fan lobe aggradation has resulted in a net westward migration of >113 km of the Kosi River over the surface of its mega-fan during the last two centuries (Wells and Dorr, 1987; Chakraborty and others, 2010). Palaeochannels are well preserved across much of the surface of the Kosi and Gandak fans (Sinha and others, 2014b), reflecting the dynamic and mobile nature of these systems. In the west Ganga Plain, the Ganga River is described as a braided channel within a narrow incised valley with exposed cliffs extending 15 to 30 m above the modern channel in parts (Shukla and others, 2001; Gibling and others, 2005; Shukla and others, 2012). Numerous phases of incision and aggradation are documented within both the Yamuna and Ganga valleys where distinct geomorphic surfaces and facies associations are preserved in exposed valley walls (Shukla and others, 2001, 2012; Gibling and others, 2005; Tandon and others, 2006).

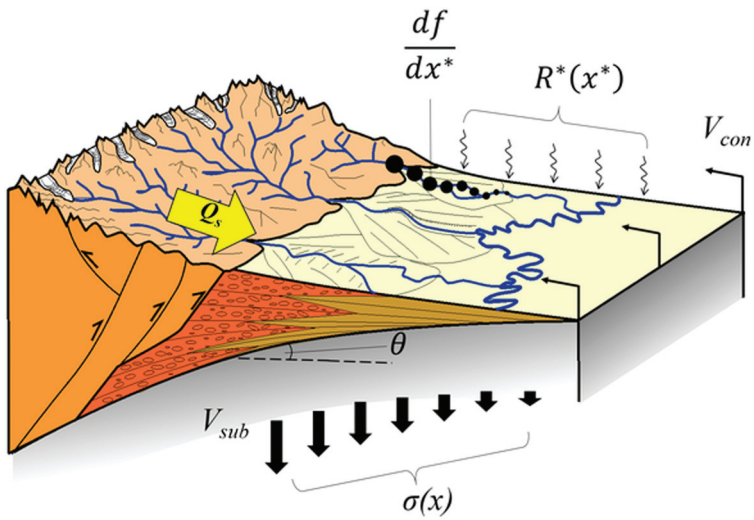

Fig. 2. Major controls on large scale channel morphology across the Ganga Plain. These controls include sediment flux, q_s, to the basin; the distribution of tectonic subsidence, $\sigma(x)$, across the basin; the spatial distribution of sediment deposition down-system, $R^*(x^*)$; sediment grain size fining rate, df/dx^*; and basin subsidence velocity, V_{sub}, which is a product of the horizontal convergence velocity across the Himalaya, V_{con}, and dip of the basement beneath the mountain front, θ.

In order to understand the controls on the variations in river morphology along the Ganga Plain, we need to consider a range of possible scenarios. As rivers exit mountain ranges, they commonly evolve into broad alluvial systems where river morphology (channel pattern, geometry, gradient) is typically determined by water and sediment discharges, sediment grain sizes, basin subsidence rates and vegetative patterns (fig. 2) (van den Berg, 1995; Dade and Friend, 1998; Dade, 2000; Marr and others, 2000; Duller and others, 2010; Allen P.A. and others, 2013). In addition, first-order predictions from various studies (for example Paola and others, 1992a; Robinson and Slingerland, 1998; Duller and others, 2010; Allen P.A. and others, 2013) are that downstream grain size trends are also controlled by sediment supply and subsidence rate, with increased sediment supply reducing fining rates, and increased basin subsidence increasing fining rates as a result of enhanced rates of deposition or aggradation promoting selective deposition in the proximal region of the basin. Grain size fining trends impact the location of the gravel-sand transition (Dubille and Lavé, 2015), and variations in river morphology (Dade and Friend, 1998).

This paper initially quantifies the basin-wide variability in incision and aggradation of the river systems across the Ganga Plain from digital topography using a swath based technique to map relative elevation of channels above or below their floodplains. The implications are that the lateral variations in incision versus aggradation should be recorded in the underlying basin stratigraphy, and that the relative contributions of sediment derived from the western and eastern Himalaya to the Ganges-Brahmaputra Delta are likely to be affected by the relative efficiency of sediment transport and bypass across the Ganga Plain. In addition to quantifying the relief along the valleys of the rivers, we also generate new basin-wide data on subsidence rates and grain size fining rates from the proximal foreland basin near to the mountain front. We finally discuss and analyze these data in context of the observed patterns in incision and aggradation of the river systems across the Ganga Plain.

A challenge when determining longer-term (millennial) controls on fluvial morphologies is to differentiate signals driven by shorter-term stochastic variations in

climate or tectonic activity in the upstream catchment (Benda and Dunne, 1997a; Tucker and Slingerland, 1997; Leeder and others, 1998). Forward models have simulated the effects of varying parameters such as sediment flux and basin subsidence over different timescales relative to the equilibrium time period of the basin, defined as the period required for streams within the basin to attain a steady-state profile (Paola and others, 1992a; Heller and Paola, 1996; Robinson and Slingerland, 1998; Marr and others, 2000). In a system as large as the Ganga Plain, potential short-term ($<10^4$ years) controls on sediment flux and grain size could be linked to climatic changes in precipitation patterns, glacial discharge and extreme storm events or earthquakes. In contrast, subsidence rates, which are controlled by topographic loading and the flexural response and subduction velocity of the underlying lithosphere (Sinclair and Naylor, 2012) are unlikely to vary at these timescales. Below, we discuss current knowledge and data available on the potential controlling parameters on the large-scale morphology of rivers across the Ganga Plain: sediment flux, basin subsidence and sediment grain size of rivers across the Ganga Plain.

Current Constraints on Sediment Flux, Basin Subsidence and Sediment Grain Size across the Ganga Plain

Our current understanding of sediment flux into the Ganga foreland basin is based principally on suspended sediment data from gauging station networks, but the spatial coverage of these data is restricted (Blöthe and Korup, 2013). Advances in detrital cosmogenic radionuclide (CRN) analysis have allowed ^{10}Be concentrations to be measured in modern river sediments, allowing approximation of average denudation rates from the source catchments over timescales of thousands of years (Vance and others, 2003; Lupker and others, 2012; Godard and others, 2014). The published CRN data give an indication of how sediment flux delivered to the foreland basin varies spatially between the major river systems that drain the Himalaya. The mean erosion rates of ~1 mm/yr derived from these data can be used to infer the timescales over which the rates are averaged, <1000 years in this case based on the reduction in CRN production rates with depth. Sediment fluxes calculated from ^{10}Be concentrations measured from the modern river sediment reveal marginally lower fluxes at the western end of the Ganga basin (fig. 3, table 1). However, estimates vary by up to a factor of three between sampling years of a single river, highlighting the difficulty in accurately quantifying sediment flux to the foreland basin using this approach (Lupker and others, 2012). Until we have a better understanding of the controls on the variability in ^{10}Be concentrations, it remains difficult to quantify spatial variations in millennial-scale sediment supply rate from Himalayan catchments. Similarly, longer term erosion rates estimated from bedrock mineral cooling ages of the Greater Himalaya Sequence along the strike of the range do not suggest a significant west to east variation in erosion rates, although rates further east are marginally (~0.5 mm/yr) higher (Thiede and Ehlers, 2013). Denudation rates over the past 4 Myr vary between ~1 to 2.5 mm/yr across the Greater Himalayan Sequence within the Ganga basin, but there are large uncertainties with these data (Thiede and Ehlers, 2013). Furthermore, erosion rates in the Greater Himalaya are thought to be relatively high in comparison to the Lesser Himalaya (Lavé and Avouac, 2001), and as such, denudation rates derived from thermochronology studies in this region do not represent catchment averaged rates. The timescales over which these denudation rates have been averaged may also be too large to reflect spatial patterns in modern or sub-millennial sediment fluxes to the Ganga Plain, and should not be interpreted as comparable rates to those derived from ^{10}Be concentrations.

Basin subsidence histories across the Indo-Gangetic Plain requires multiple, well documented wells with good stratigraphic resolution (Allen P.A. and Allen J.R., 2013), but these types of data are not available for this region (Burbank and others, 1996).

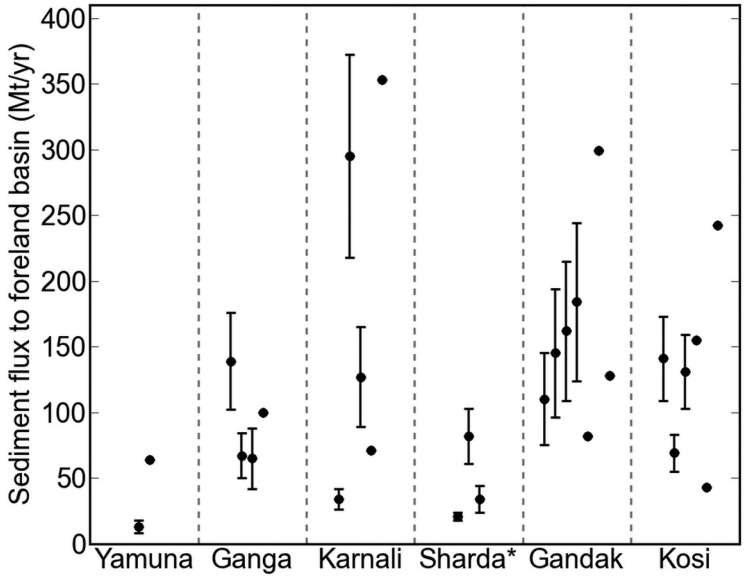

Fig. 3. Sediment flux estimates derived from cosmogenic ^{10}Be concentrations (and errors) and suspended sediment concentrations. (*) Where no data were available for the Sharda catchment, catchment-averaged erosion rates derived from the adjacent Karnali catchment (from Lupker and others, 2012) were used to calculate sediment flux estimates.

Therefore, for this study, we calculate the tectonic forcing of subsidence using the depth to the crystalline basement that underlies the Siwalik succession derived from the Seismotectonic Atlas of India, prepared by the Geological Survey of India (Narula and others, 2000), integrated with the local subduction velocities (Sinclair and Naylor, 2012).

Grain size data from the principal Himalayan rivers are not available, and are therefore a key component of the new data presented in this study. We note that detailed downstream grain size fining trends have been analyzed from smaller Himalayan rivers (Dubille and Lavé, 2015) that drain the foothills termed 'Piedmont Rivers' (Sinha and Friend, 1994). The grain size data show a clear transition from gravel to sand in the rivers at approximately 8 to 20 km from the mountain front. Given the order of magnitude increase in catchment size and likely sediment supply from the larger rivers that drain the high mountains of the Himalaya, it is reasonable to predict an increase in distance from the mountain front to the gravel-sand transition for the main rivers presented here.

REGIONAL CONTEXT

The Himalayan foreland basin formed as a result of the ongoing collision between the Indian and Eurasian plates, where crustal thickening generates high topography that is supported by the flexural rigidity of the underlying lithosphere (Lyon-Caen and Molnar, 1985; Flemings and Jordan, 1989; Burbank and Beck, 1991; Burbank, 1992; Brozovic and Burbank, 2000). Along the strike of the mountain range, variations in lithospheric rigidity and basement faulting are believed to have modulated both basin width and large-scale patterns of subsidence (Burbank and others, 1996). The Himalayan orogen is split into four major structural units that run broadly parallel from west to east (fig. 1). These units are from south to north: the Neogene Siwalik Group, the Proterozoic Lesser Himalayan Sequence, the Proterozoic-Ordovician Greater Himala-

TABLE 1

Sediment flux estimates summarized from Blöthe and Korup (2013)

River name	Sediment flux (Mt yr^{-1}) at mountain front	Source
Yamuna	13±5	Lupker and others, 2012*
	64	Jha and others, 1993***
Ganga	139±37	Lupker and others, 2012*
	67±17	Vance and others, 2003*
	65±23	Vance and others, 2003*
	100	Wasson, 2003***
Karnali	34±8	Lupker and others, 2012*
	295±77	Lupker and others, 2012*
	127±38	Lupker and others, 2012*
	71	Ghimire and Uprety, 1990***
	353	Andermann and others, 2012**
Gandak	110±35	Lupker and others, 2012*
	145±49	Lupker and others, 2012*
	162±53	Lupker and others, 2012*
	184±60	Lupker and others, 2012*
	82	Sinha and Friend, 1994***
	299	Andermann and others, 2012**
	128	Ghimire and Uprety, 1990***
Kosi	141±32	Lupker and others, 2012*
	69±14	Lupker and others, 2012*
	131±28	Lupker and others, 2012*
	155	Ghimire and Uprety, 1990***
	43	Sinha and Friend, 1994***
	242	Andermann and others, 2012**

* Sediment flux derived from ^{10}Be concentration in sand.
** Based on a mean daily suspended sediment flux (1973-2006).
*** Suspended sediment concentration.

yan Crystalline Complex and the Proterozoic to Eocene Tethyan Himalayan Sequence (Yin, 2006). These lithological units are bound by major faults, the most active of which is the Main Frontal Thrust (MFT). The MFT is the most southerly structure, situated between the Siwalik Group and the foreland basin, and absorbs approximately 80 percent of the ~21±1.5 mm/yr convergence) between India and south Tibet in central Nepal (Lavé and Avouac, 2000).

Sediment generated by the erosion of the Himalayan mountain range accumulates in the foreland basin. The thickness of the basin fill reduces progressively with distance from the mountain front, consistent with asymmetric subsidence caused by thrusting of the overlying orogen (Burbank and Beck, 1991; Burbank, 1992; Yin, 2006). The basin fill is dominated by the Neogene Siwalik Group and the pre-Miocene Rawalpindi Group (Burbank and others, 1996). The Siwalik Group comprises thick molasse deposits formed by the erosional products of the Lesser and Higher Himalaya (for example Kumar and others, 2004). Thin-skinned tectonics associated with the MFT have incorporated these poorly consolidated molasse deposits in the hanging wall

of frontal structures, forming the Siwalik Hills which represent the youngest and southernmost topography of the Himalaya (Mugnier and others, 1999). The foredeep basin (*sensu* DeCelles and Giles, 1996) lies immediately south of the Siwalik Hills, forming the Indo-Gangetic Plain. Immediately inboard of the thrust front are several wedge-top basins, locally termed 'Duns' that act to buffer the sediment delivery to the foredeep (Densmore and others, 2016). In comparison to the confined bedrock channel both upstream and downstream of the Dun, the laterally unconfined and lower gradient surface of these Dun valleys has promoted sediment deposition during periods of heightened sediment export from the mountains, producing a thick alluvial valley fill. Dun valleys of direct relevance to this study are the Chitwan and Dehra Dun valleys where the Gandak, Ganga and Yamuna rivers flow through prior to passing the MFT and exiting onto the Plain (fig. 1).

The Ganga Plain (and henceforth Plain) forms the central third of the Indo-Gangetic Plain and covers an area of 250,000 km^2, whilst the drainage area of the entire Ganga basin is in excess of 1,060,000 km^2 (Singh, 1996). The hydrology of rivers draining the basin is dominated by the Indian Summer Monsoon (ISM), when over 85 percent of the annual rainfall falls between June and September (Sinha and Friend, 1994; Tandon and others, 2006), producing broad peaked annual hydrographs. Along strike gradients in precipitation have been identified using passive microwave data (Bookhagen and others, 2005; Anders and others, 2006) where catchments in the east typically experience more Indian summer monsoon precipitation than those in the west. A strong north-south precipitation gradient has also been identified as a result of orographic enhancement of precipitation, where the heaviest rainfall is induced by the first significant topography encountered by southerly air masses originating from the Bay of Bengal (Bookhagen and others, 2005; Bookhagen and Burbank, 2006; Anders and others, 2006). Apatite fission track ages from across the entire Himalaya do not reveal any systematic change in exhumation rates along the strike of the range (Thiede and Ehlers, 2013).

Sediment carried into the foreland basin that is not immediately deposited, typically sand and finer material, can continue downstream via the Ganga, Brahmaputra and Indus rivers ultimately reaching the sea where it accumulates in the Bengal and Indus fans. This fraction represents up to ~90 percent of the total sediment load exported from the Himalaya (Lupker and others, 2011). Sediment trapped within the foreland basin is deposited across vast alluvial fans that are separated by broad interfan or interfluve areas that are drained by foothill or Plain fed rivers (Jain and Sinha, 2003; Sinha and others, 2005). These interfan parts of the basin are filled primarily with sediments eroded from the frontal Siwalik range, and sediments derived and reworked locally from the Plain (Sinha and others, 2005).

The rivers feeding the Plain can be divided into mountain, foothill and Plain fed (Sinha and Friend, 1994). Mountain-fed rivers originate from large source areas within the Himalayan orogen, typically with a glacial source. Foothill or 'Piedmont' rivers have relatively small catchment areas of 20 to 2500 km^2 (Dubille and Lavé, 2015) and drain the interfluve region between alluvial fans created by sediment deposition of the much larger mountain fed rivers. Plain fed rivers repetitively rework sediment deposited by the mountain and foothill fed rivers (Sinha and others, 2005). Grain size measurements in central Nepal across a number of interfan or foothill fed channels have documented a rapid gravel-sand transition occurring ~8 to 20 km downstream of the mountain front (Dubille and Lavé, 2015). This same rapid transition is consistent with vertical grain size measurements taken from the Siwalik molasse exposed in the frontal Himalayan folds (Dubille and Lavé, 2015). Grain size fining rates have not been documented for the mountain fed rivers.

METHODOLOGY

Topographic Analysis

Effective mapping of channel elevations relative to their adjacent alluvial fan surface reveals spatial variations in both aggradation and incision of active fluvial systems. Existing approaches to identify regions where channels are perched above their adjacent floodplain, or 'super-elevated' (Bryant and others, 1995), are typically limited to linear elevation transects across target alluvial fans using digital elevation models (DEMs) (for example Sinha and others, 2005; Chakraborty and Ghosh, 2010; Chakraborty and others, 2010). A number of limitations arise from this approach: (i) the approach is limited in its spatial resolution as each transect only records elevation across a small portion of the fan, which may not necessarily be coincident with areas of highest avulsion risk; (ii) the orientation of the transects does not directly reflect the geometry of either the channel or fan system; (iii) differentiating data noise from geomorphic features such as channel levees that are often comparable in amplitude (Chakraborty and others, 2010), requiring significant degrees of smoothing to pick out first order features of the alluvial fan system (Chakraborty and Ghosh, 2010). Sinha and others (2014a) addressed the first of these issues by taking a series of profiles following parallel linear transects at 2 km spacing down the Kosi fan, permitting an assessment of changes in channel super-elevation along the length of the alluvial fan; however, the spatial resolution is still limited to the transects themselves, and suffers from the same problems relating to transect orientation and noise outlined above. Noise reduction could potentially be achieved using swath profiles which provide a means of increasing the signal-noise ratio, and should highlight characteristics of the along-profile topography (Telbisz and others, 2013; Hergarten and others, 2014). More recent generalized swath profile methods permit the use of arbitrary, non-linear baselines, such as river courses, enabling the unbiased characterization of river valley morphology, but averaging along the length of a stream reach, reducing resolution (Hergarten and others, 2014).

We present a new, spatially distributed method to map patterns of fluvial incision and aggradation across alluvial fan systems that addresses the above issues. The premise of this method is that when a channel is elevated relative to its floodplain or adjacent fan surface, the adjacent surface will lie below the elevation of the channel; when incised, the adjacent surface will have a higher elevation relative to the channel. Therefore, by mapping every location within the DEM to the closest point in the channel, it is possible to assess the relative elevation of the channel compared to the rest of the fan.

In order to produce maps of channel super-elevation, we use a swath-based method, similar to that developed by Hergarten and others (2014) to construct generalized swath profiles using curvi-linear baselines.

The first step in our procedure is to extract the trunk channel on the alluvial fan from the DEM. For this work, river networks were extracted from a 90 m resolution Shuttle Radar Topography Mission (SRTM) DEM using ESRI ArcMap v10.1, using a steepest-descent flow routing algorithm. Channel elevations along these river networks represent the elevation of the water surface in 2000, the time of the SRTM data capture. The root mean squared error (RMSE) of these data in mountainous regions is ± 7.75 m, while in less mountainous regions, the RMSE of the SRTM is ± 14.48 m (Amans and others, 2013). Given that the flow stage will be highly variable through the year, there may be a small impact on these results, although this is likely to be within the RMSE error of the DEM. As such, the use of these data should provisionally be limited to the interpretation of very large scale patterns or where relief exceeds the RMSE of the data ($\sim \pm 10$–15 m).

These trunk channels are subsequently used as a baseline along which we generate an 80 km wide swath. This swath determines the region in which we map the relative super-elevation of the trunk channel, and in other applications can be modified for other river systems as required. Within this neighbourhood, we iterate through every pixel, p_i, and map it to the nearest point in the trunk channel baseline, following Hergarten and others (2014); DEM pixels for which the closest point on the baseline is at either of the termini are excluded. The elevation difference between the fan surface and the nearest point on the trunk channel is then calculated, with the resultant swath revealing spatial variations in the elevation of the fan surface relative to the closest point in the active channel (fig. 4). Negative values indicate areas of the fan that are lower in elevation to the closest point in the trunk channel (the channel is perched above the neighboring fan surface); these areas are shaded red on the swath in figure 4. Conversely, where the trunk channel is entrenched, elevations on the neighboring fan surface are greater than the closest point in the trunk channel; the more entrenched portions of the swath are colored in blue on figure 4. Areas of the swath that are at a similar elevation to the channel are shaded in yellow, and areas more than 100 m above the channel are in purple, which typically represents mountainous topography.

Channel lengths extending from the Himalayan mountain front (defined as the most southerly area of notable relief) to the Ganga trunk stream were extracted for each river. Longitudinal profiles of each river were also extracted from the DEM from which slope values averaged over a 10 km moving window were then calculated. Normalized channel steepness (k_{sn}) was also calculated at the fan apex using a reference concavity of 0.5, to allow comparison of channel gradients independently of upstream catchment area (Wobus and others, 2006; Allen G.H. and others, 2013). Similar profiles were constructed from the surface of the adjacent floodplains, or valley tops where channels were entrenched in the west Ganga Plain. These profiles followed transects that were broadly parallel to the channel.

Basin Subsidence

The distribution of sediment deposition, or the spatial apportioning of sediment sorting, at a given distance (x) can be expressed as:

$$R(x) = \frac{r}{q_s} \tag{1}$$

where r is the rate of sediment deposition, and q_s is sediment flux (Paola and Seal, 1995). R can be made non-dimensional such that:

$$R^*(x^*) = C_0 \frac{r(x)}{q_s(x)} L \tag{2}$$

where R^* is the non-dimensional function that describes the distribution of deposition, C_0 is the volumetric sediment concentration on the bed, r is the rate of sediment deposition, q_s is the sediment flux, and L is the length of the depositional stream (Paola and Seal, 1995). Assuming that the rate of sediment deposition is controlled by the rate of tectonic subsidence, defined as $\sigma(x)$, $R^*(x^*)$ can also be expressed as:

$$R^*(x^*) = (1 - \lambda_p) L \frac{\sigma(x)}{q_s(x)} \tag{3}$$

where L is the length of the depositional stream, $q_s(x)$ is the rate of decay in sediment flux downstream ($L\ t^{-1}$), λ_p is the sediment porosity and x^* is the normalized longitudinal location along a deposition system of length L (Duller and others, 2010).

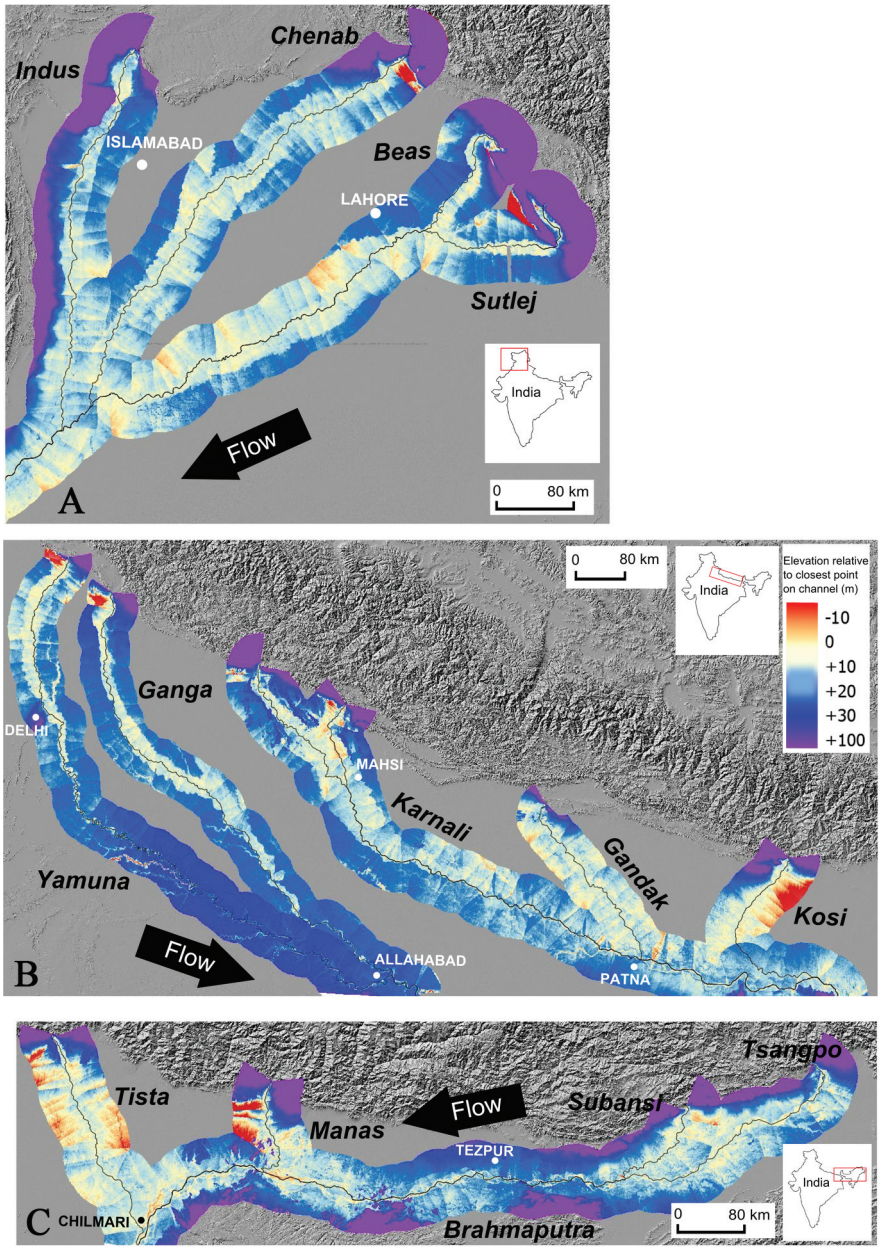

Fig. 4. Valley topography from swath profile analysis for the three major river basins across the Himalayan foreland basin from west to east; (A) Indus (B) Ganga and (C) Brahmaputra.

If R^* determines how sediment sorting is apportioned spatially, most sorting will occur at the upstream end of the system where the greatest proportion of sediment is deposited (Duller and others, 2010). The rate of down-system grain size fining can also be described by the fractional Exner sediment mass balance (Paola and Seal, 1995), also incorporating tectonic subsidence through the R^* function:

$$\frac{df}{dx^*} = f\left[R^*\left(1 - \frac{1}{J}\right)\right] - \frac{1}{J}\frac{dJ}{dx^*} \tag{4}$$

where f is the fraction of a given sediment size in the deposit and $J = p/f$, where p is the fraction of a given sediment size in the transporting system (Duller and others, 2010). This predicts a correlation between subsidence rates, sediment grain size fining rate and hence river morphology.

The methodology for calculating the tectonic forcing of subsidence of the surface near the mountain front uses new maps of the depth to crystalline basement derived from seismic data combined with known shortening rates (Stevens and Avouac, 2015). The approach doesn't use the depth to basement, but instead utilizes the gradient of the basement nearest to the mountain front (Sinclair and Naylor, 2012). By reconstructing the gradient of the basement of the subducting slab (θ) and combining it with known convergence velocities (V_{con}) between the Ganga Plain and the Himalaya (Stevens and Avouac, 2015), we can derive the vertical velocity which determines the modern subsidence velocity at the surface (V_{sub}) at point x using:

$$V_{sub}(x) = V_{con}\ tan\ \theta(x) \tag{5}$$

This tectonic forcing of surface lowering (subsidence) at the mountain front remains steady as long as the following remain constant: 1) the mean distribution and magnitude of topography; 2) the density structure of the mountain range; 3) the convergence velocity between the subducting lithosphere and the distributed load of the range, and 4) the gradient of the subducting lithosphere. Within these parameters, the most likely to vary at a high spatial and temporal scale is the distribution of topography, as thrust units are accreted at the front of the range. Analogue and numerical experiments from thrust wedges indicate that fluctuations in frontal accretion versus internal thickening of the wedge can result in punctuated topographic growth at a timescale characterized by the length of accreted thrust sheets divided by the convergence velocity (Hoth and others, 2007; Naylor and Sinclair, 2007). For the Himalayas, typical spacing of thrust units are approximately 12 km, which when divided by a mean convergence velocity of 18 km/Myr yields a timescale of probable topographic variations of 0.66 Myr.

Additionally, the rate of stratigraphic onlap of the Siwalik Group onto the basement of the foredeep is 19±5 km/Myr which is comparable to the convergence velocity, suggesting these parameters have been in steady state for the recent history of the thrust wedge and foreland basin system (Lyon-Caen and Molnar, 1985; Mugnier and Huyghe, 2006). Based on these arguments, we do not envisage the tectonic forcing of subsidence to have varied significantly for at least the last 100,000 years.

For this study, the time interval of interest is the period over which the present morphology of the river systems of the Ganga Plains is defined; this interval may be approximated by the topographic relief of the fluvial system divided by the sediment accumulation rates. In this case, the local relief of the incised and super-elevated channel systems is up to 30 m. Holocene sedimentation rates for the proximal basin are of the order of 1 mm/yr (Sinha and others, 1996). Based on these rates, we propose that the time interval of interest in determining the basin's surface morphology is approximately 30,000 years. Consequently, we see no reason to consider that subsidence rates have varied at any given location in the basin during the development of the present-fluvial morphology across the Ganga Plain.

The long-term ($>10^6$ yr) and recent convergent velocity between the subducting plate and the Himalayan topography can be approximated from the stratigraphy of the foreland basin, and modern GPS data respectively. As outlined above, stratigraphic sequences observed in deep well and seismic data imply convergence rates of between

~10 to 20 mm/yr over the past 15 to 20 Ma from these data (Lyon-Caen and Molnar, 1985). Contemporary GPS data (Feldl and Bilham, 2006; Stevens and Avouac, 2015) have demonstrated along strike differences in modern India-Tibet convergence rates. Rates in the eastern Himalayan arc are typically 18 to 20 mm/yr compared to 12 to 15 mm/yr in the west. The tectonic displacement of fluvial terrace surfaces in central Nepal (Lavé and Avouac, 2000) and northwest India (Wesnousky and others, 1999) further support a systematic east to west decrease in convergence rates with estimates of 21.5±1.5 mm/yr and 11.9±3.1 mm/yr, respectively.

Models calibrated against gravity data have also indicated that the flexural rigidity of the Ganga Basin varies along strike of the basin (Lyon-Caen and Molnar, 1985; Jordan and Watts, 2005). Jordan and Watts (2005) demonstrated that the central Himalayan foreland basin, which relates to the west Ganga Plain, has a higher effective elastic thickness (~70 km) compared to regions in the east and west (~30–50 km).

The gradient of the basement beneath the proximal foreland basin (θ) is measured using the depth to basement plots of the Ganga basin derived from depth converted reflection seismic data (fig. 5A). The dip of the basement beneath the mountain front has been calculated using the average gradient of the first 30 km of each profile basin-ward of the mountain front, thus reflecting a control on basin subsidence velocities of the proximal basin. Six cross-sections of the foreland basin have been generated from these plots and second order polynomial equations and curves have been fitted through the data to extend the cross section to a point beneath the mountain front to account for increasing rates of subsidence close to the mountain front (Sinclair and Naylor, 2012). A range of V_{sub} values have been calculated along the course of each river using variable V_{con} values to assess the impact on V_{sub} estimates. The variable convergence rate estimates used are based on Stevens and Avouac (2015) with values of 13.3±1.7 mm/yr for the Yamuna and Ganga, 18.5±1.8 mm/yr for the Sharda and Karnali and 20.2±1.1 mm/yr for the Kosi and Gandak. Previously mentioned convergence rate estimates from Wesnousky and others (1999) and Lavé and Avouac (2000) have also been included in this analysis.

Grain Size

Extensive coarse gravel bars dominate the bed of the major rivers of the Ganga Plain as they exit the mountain front. During the low-flow season (October-May), a considerable portion of the channel bed is accessible. If it is assumed that equal mobility conditions (Parker and Toro-Escobar, 2002) are attained during monsoon flows, allowing full reworking of gravel bar material, then the gravel deposits visible during this period should represent bedload transported and deposited during the preceding monsoon (Attal and Lavé, 2006). Equal mobility implies that the grain size distribution of the annual transported yield is finer than that of the gravel in the armored surface exposed at low flow, and similar to that beneath the armored layer in the subsurface (Parker and Toro-Escobar, 2002). Grain size measurements were taken from ~30 to 50 km upstream of the mountain front down to the gravel-sand transition of each of the Kosi, Gandak, Sharda, Ganga and Yamuna rivers. Ideally, measurements would have been carried out at regular intervals but sampling was restricted by access and in-channel structures. Where large engineered dams (barrages) have been constructed to divert water into channels for irrigation were present, samples were taken at least 1 to 2 km upstream or downstream of the structure to minimise localized hydrodynamic and trapping effects, this being the distance over which the influence of the barrage appeared to dissipate.

Grain size measurements were taken of both the surface and subsurface material using photographic and volumetric analysis, respectively, to account for the effects of surface coarsening (Dietrich and others, 1989; Parker, 1990). Samples were restricted to parts of the bar which appeared recently reworked with imbricated and sub-rounded

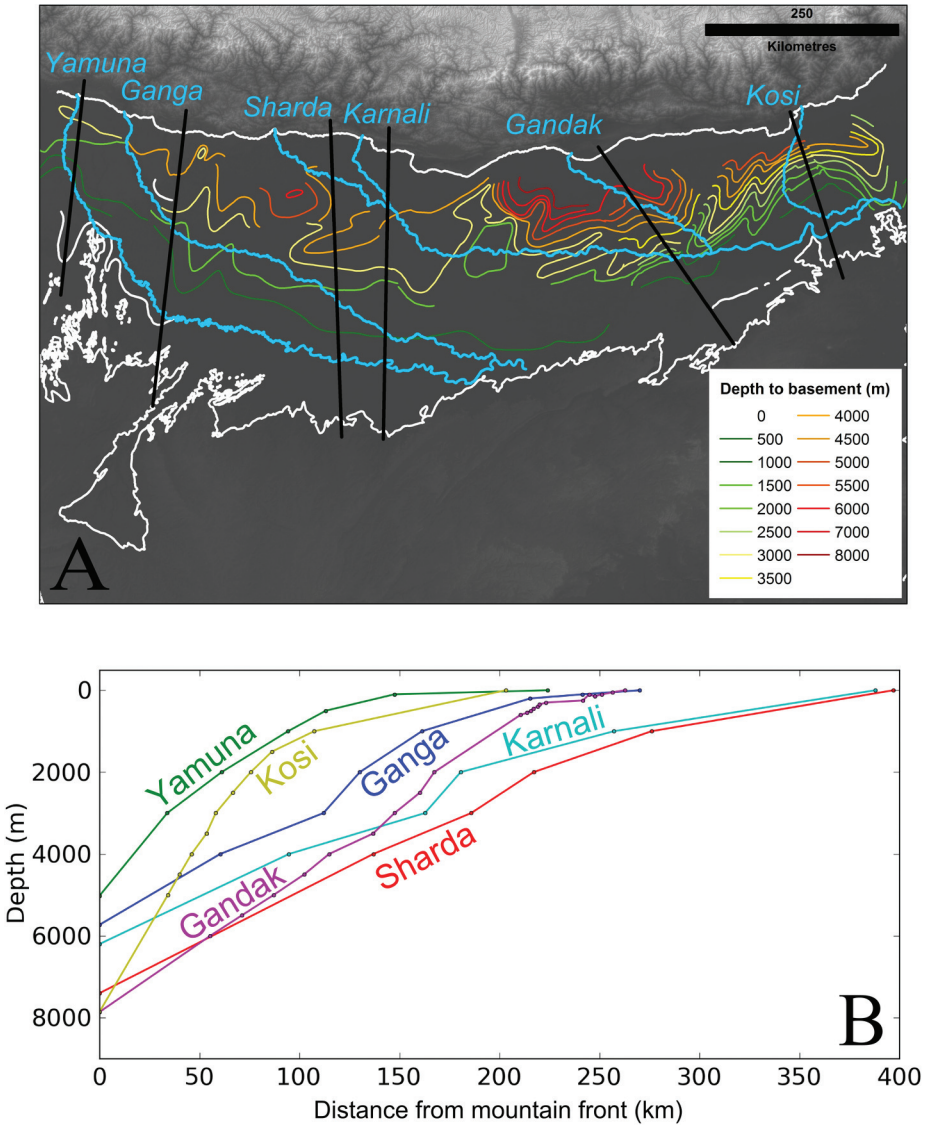

Fig. 5. (A) Depth to basement contours across the Ganga basin showing positions of basin cross sections (black line) for each river and (B) basin profiles constructed using depth to basement contours in proximity of the Yamuna, Ganga, Sharda, Karnali, Gandak and Kosi rivers. Data sources: 90 m SRTM DEM and Geological Survey of India.

to rounded gravel (clearly fluvial in origin). Gravel size variations were observed down the length of the gravel bars so sites were chosen in the centre of the coarsest fraction for consistency. At each site, 5 to 10 photos were taken of the channel bed to use for photo counting. Particle sizes were measured from each photo by overlaying a regular numeric square grid with 100 nodes, and measuring the intermediate *b*-axis of each pebble beneath the nodes (Attal and Lavé, 2006; Whittaker and others, 2011). Due to the coarse nature of much of the gravel bars, larger pebbles were often covered by multiple grid intersections. Consistent with the sampling method of Attal and others

(2015), pebbles covering n grid intersections were counted n times. This premise is based on Kellerhals and Bray's analysis (1971) using a voidless cube model, although it is noted that this method results in over estimation of D_{84} values (Attal and others, 2015). Results from each photo at a given site were combined to create a single grain size distribution at each sampling location.

Volumetric subsurface measurements were taken using techniques documented by a number of studies (Attal and Lavé, 2006; Whittaker and others, 2010; Dubille and Lavé, 2015). Surface material was first removed from the site location (to a depth equal to the size of the largest pebble) and 100 to 300 kg of material was excavated and sieved through a series of 1, 2 and 4 cm square mesh sieves. Pebbles larger than 8 cm were individually weighed, and the weight of each fraction was recorded. For pebbles with *b*-axis greater than 8 cm, a representative diameter was calculated by assuming that the pebble was roughly spherical and had a density of 2650 kg m^{-3} (Whittaker and others, 2010). A well-mixed representative sample of ~1 kg of the fraction < 1 cm was sieved using a 1 mm sieve, from which a ratio was calculated and applied to the whole <1 cm fraction.

The presence of boulders on some gravel bars meant that the recommendation that the largest clast represents < 5 percent of the sample mass was not always fulfilled (Church and others, 1987). For both surface and subsurface measurements, the effects of excessively large pebbles on D_{84} and D_{50} measurements was assessed using the same method outlined in Attal and others (2015). This process involves the removal of the largest clast from the distribution and recalculating the D_{84} and D_{50} values. This process was then repeated but with the addition of a large clast, similar in mass to the largest clast recorded within that sample. The recalculated D_{84} and D_{50} values with the removal or addition of the largest clast are plotted as upper and lower error bars on subsurface volumetric samples. Due to the large number of measurements obtained for each surface sample, following the same procedure on surface grain size distributions produced minimal variation (< 5%) in D_{84} and D_{50} values. Instead, a more conservative approach was taken, as outlined in Whittaker and others (2011), where an error margin of ±15 percent was applied to account for subjective bias when measuring the intermediate axis of each pebble beneath the grid node. This margin of 15 percent was estimated by Whittaker and others (2011) based on the differences in grain size distribution from repeat sampling of the same photo.

The position of the gravel-sand transition was also mapped for each river, by noting the point at which exposed deposits were near exclusively sand (> 95%). In some instances, small patches of gravels were present but represented a very small proportion (~1–5 %) of the bed fraction based on visual observations.

Downstream fining rates of the gravel fraction along each river were calculated using Sternberg's exponential function of the form:

$$D_x = D_0 e^{-\alpha x} \tag{6}$$

where D_0 is the predicted input or initial characteristic grain size in the system (such as D_{84}), α is the downstream fining exponent and x is the distance downstream (Sternberg, 1875). Linear functions have also been fitted to account for alternative fining patterns observed in the literature (Rice, 1999; Whittaker and others, 2011):

$$D_x = D_0 - \beta x \tag{7}$$

where β is the dimensionless fining rate (grain size reduction/km). The two key processes that are commonly seen to control downstream fining rates in fluvial systems are (1) the selective transport and deposition of particles and (2) abrasion of particles where larger particles are broken down by mechanical processes (Paola and others, 1992b, 1992a; Ferguson and others, 1996; Rice and Church, 2001; Attal and Lavé, 2006;

Fedele and Paola, 2007; Duller and others, 2010). The effect of pebble abrasion is considered negligible in this instance, as the lithology of gravel bars in all rivers was dominantly quartzite, suggesting that grain size fining by abrasion is likely to be similar across all systems. Any differences in grain size fining will likely reflect spatial variations in the grain size distribution of sediment delivered to the Plain from the Himalaya, sediment flux, the spatial distribution of basin subsidence, and local hydraulic and topographic effects (Paola and others, 1992a; Robinson and Slingerland, 1998; Fedele and Paola, 2007; Duller and others, 2010; Whittaker and others, 2011).

RESULTS

Topographic Analysis

Along the strike of the mountain front, results of the swath profile analysis are consistent with previous findings (Gibling and others, 2005; Sinha, 2005; Sinha and others, 2005) where the degree of channel entrenchment was found to increase from east to west (fig. 4). In the far west of the Ganga Plain, both the Yamuna and Ganga rivers are clearly entrenched within well-defined broad valleys that are incised into the surface of their respective alluvial fans. These incised valleys narrow with distance downstream of the mountain front from ~20 km to < 1 km at a point immediately upstream of the Ganga and Yamuna confluence at Allahabad (fig. 4B). Close to the mountain front, the valley sides are ~30 m high and reduce to 10 to 20 m by ~80 km downstream. Lateral incision into valley walls by large meander loops are clearly preserved in the lower half of the Ganga River. The Sharda and Karnali rivers converge at Mahsi, ~100 km downstream of the mountain front, to form the Karnali system which is also known as the Ghaghara River in India (fig. 4B). Both tributaries of the Karnali River flow down a well-defined incised valley up to 40 km in width. Downstream of the Sharda and Karnali confluence, the river course turns more sharply to the east and the incised valley loses definition as the degree of entrenchment into the fan surface is reduced. Much of the surrounding floodplain is of a comparable elevation (within 10 m) to the active channel here. Further east, the Gandak and Kosi rivers show minimal signs of entrenchment on the surface of their respective alluvial fans. Much of the surrounding floodplain is of a similar or lower elevation, most notably on the Kosi River (Chakraborty and others, 2010; Sinha and others, 2013; Sinha and others, 2014a).

The Kosi channel currently occupies the western margin of its alluvial fan where the channel bed is marginally elevated with respect to the surface of the central area of the fan. This pattern is most apparent in the upper ~80 km of the fan where much of the floodplain on the east bank is relatively lower in elevation, in some cases by up to nearly 10 m, than the active channel (fig. 4A). Whilst still within the RMSE of the DEM, this observation appears consistent with independent observations. In 2008 the Kosi River breached its eastern embankment at Kusaha, Nepal (Sinha and others, 2009; Chakraborty and others, 2010). Much of the avulsion belt occupied the depressed area identified as lower in elevation in the SRTM data that were captured several years earlier in 2000. For the remaining length of the fan, the Kosi channel sits at a very similar elevation to that of the fan surface.

This west to east gradient also extends beyond the Ganga Basin into the wider Indo Gangetic Plain. East of the Ganga Plain, tributaries of the Brahmaputra River appear similar in nature to the Gandak and Kosi rivers where channels are either at a similar elevation or marginally super-elevated relative to their surrounding floodplain (fig. 4C). Further west, rivers in the Indus basin show similar characteristics to those in the west Ganga Plain where active channels are laterally constrained in broad incised valleys (fig. 4A). Unlike the Ganga Plain however, these valleys widen with distance downstream and the degree of entrenchment appears lower at 10 to 20 m. This is

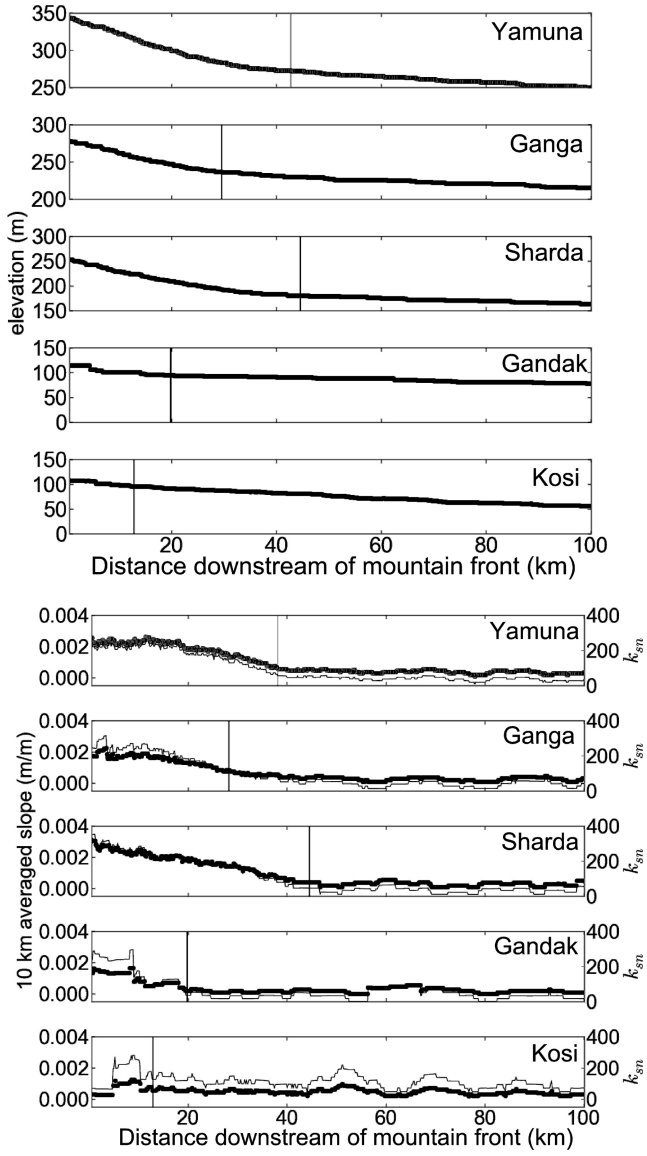

Fig. 6. Longitudinal profiles, 10 km averaged slope and normalized channel steepness (k_{sn}) values for major tributaries of the Ganga basin. k_{sn} values are shown by the thinner black line on the slope plots. Vertical lines represent the position of the mapped gravel-sand transition.

interpreted as a contrast in dominant controls on channel morphology between the Indus and Ganga basins.

Longitudinal river profiles and 10 km averaged slope values extracted from SRTM data show that the Yamuna, Sharda and Karnali rivers exhibit elevated slope values relative to rivers further east within the first 40 km downstream of the mountain front (fig. 6). The Ganga however appears to exit the mountain front with a marginally lower gradient than the other west and central Ganga Plain rivers. In the east Ganga Plain the Gandak and Kosi rivers are lower in gradient, with maximum values of ~0.0015 m/m

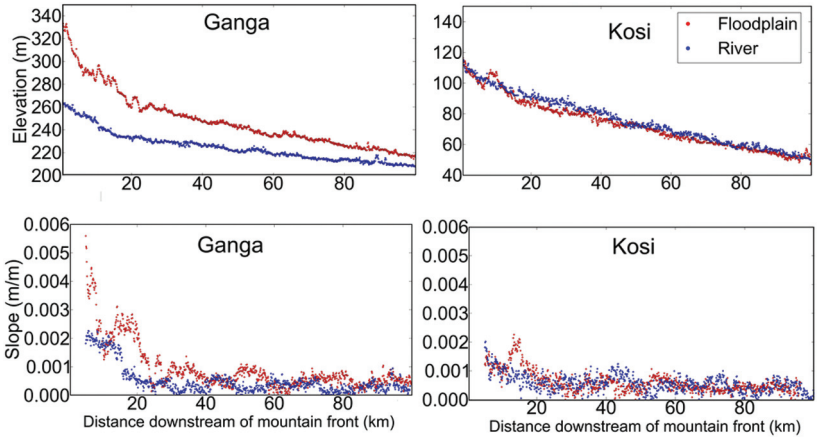

Fig. 7. Absolute elevation and 10 km averaged slope values of the modern Ganga and Kosi channels and their adjacent fan surfaces at the fan apex. Fan surface profiles followed transects that were broadly parallel to the channel, either from the top of the valley side where channels were entrenched or within ~5 km of the modern channel.

in the first 10 km, rapidly decreasing to ~0.0005 m/m by 20 km downstream of the mountain front. The Kosi maintains a more consistent and initially lower gradient down the length of its fan, attaining a maximum value of ~0.001 m/m. By 40 km downstream, all of the channel gradients converge at ~0.0005 m/m and fluctuate between 0 to 0.001 m/m for the remainder of the profile (fig. 5B). By normalizing channel gradient for upstream catchment area (k_{sn}), similar patterns are displayed where systems in the west and central Ganga Plain are typically steeper at the fan apex, with k_{sn} values of 200 to 300 (fig. 6). Whilst both 10 km averaged slope and k_{sn} values appear to be influenced by some noise along the first 10 km of the Gandak and Kosi profiles, k_{sn} values in the east Ganga Plain appear slightly lower (150–250). With the exception of noise in the Gandak profile, there were no evident knickpoints that were larger in magnitude than the RMSE (~15 m) of the data.

Comparing the average gradient of the Ganga and Kosi channels to their adjacent fan surfaces, we see that the Ganga fan surface is steeper than the active channel (fig. 7). This is more pronounced at the fan apex where the degree of channel entrenchment is also greatest. In contrast, the surface gradient of the Kosi fan is comparable to the gradient of the active channel, and an absence of significant channel entrenchment is also clearly highlighted.

Basin Subsidence

The depth to basement plots (fig. 5B) demonstrate an along strike variation in the geometry of the Ganga basin, as has also been recognized previously by Singh (1996). In the east Ganga Plain, the basin is deeper (5000–6000 m) and relatively narrow at ~200 km. The basement has a steep or even convex, distal edge. Further west, the basin widens beneath the Sharda and Karnali rivers. Generally, the basin is shallower here but there are isolated basement lows such as on the Sharda section where the basin reaches 6000 m near to the mountain front. In the far west, the basin is notably shallower at 3000 to 4000 m and again narrows to ~200 km wide. These variations in depth to basement at the mountain front broadly correlate with the variations in flexural rigidity of the downgoing lithosphere (Jordan and Watts, 2005), with lower rigidities correlating with greater basin depth at the mountain front.

Results indicate that the highest average subsidence velocities (V_{sub}) at the mountain front are located in the east of the region near the Kosi fan, with rates of 1.6±0.6 mm/yr. Further west average subsidence rates decrease to 1.4±0.4 mm/yr beneath the Gandak, 0.4±0.2 mm/yr beneath the Karnali, 0.8±0.2 mm/yr beneath the Ganga, and 0.3±0.4 mm/yr beneath the Yamuna. V_{sub} estimates are generally comparable across all but the Kosi and Gandak systems, which are notably higher. When these calculated subsidence estimates are compared to documented short term sedimentation rates across the Ganga Plain, values are comparable. An average sedimentation rate of ~0.08 (±0.19) mm/yr for the entire Ganga floodplain has been calculated from chemical mass balance equations (Lupker and others, 2011). Sedimentation rates would be expected to increase exponentially from the cratonic to orogenic margin of the basin however (Flemings and Jordan, 1989), which is consistent with sedimentation rates documented closer to the mountain front. Sedimentation rates of 0.62 to 1.45 mm/yr have been calculated from radiocarbon dating of organic material in northern Bihar upstream of the axial Ganga channel between the Kosi and Gandak rivers, averaged over a time period of 700 to 2500 yr (Sinha and others, 1996). The comparison of calculated long term subsidence rates of 1.6±0.6 mm/yr beneath the Kosi fan with the short term sedimentation rates of 0.62 to 1.45 mm/yr suggest the system is broadly in balance, with subsidence slightly outpacing sediment accumulation in this part of the basin.

Grain Size

Grain size distributions from sites closest to the mountain front have been compared across each of the sampled channels and are found to be comparable between systems (fig. 8). Subsurface grain sizes documented close to the mountain front on the Yamuna are generally finer than other sites, where a D_{84} value of 66 mm was recorded compared to values ranging between 146 to 248 mm for the Kosi, Sharda and Ganga. This is attributed to the upstream barrage near Faizabad (~3 km upstream). Compared to similar barrages located close to the mountain front on the Ganga, Sharda and Gandak rivers, a much larger proportion of flow is diverted into extensive canal networks at the Yamuna barrage, resulting in severely reduced flows downstream in the natural channel. During low flow conditions, parts of the Yamuna channel are entirely dry. It seems reasonable to interpret that a greater proportion of coarser material is trapped upstream or very close to the barrage, where there is insufficient discharge to rework or mobilise the coarsest fraction. The D_{84} of the subsurface Gandak sample was also found to be relatively fine (83 mm) compared to the Kosi, Sharda and Ganga samples, which is likely a function of the upstream Chitwan Dun. The coarse fraction of the sediment load is likely to be deposited at the upstream edge of the Dun, where bedrock channels emerge onto the low gradient alluvial surface of the Dun. This is consistent with grain size measurements taken within the Dun which show an overall fining and narrowing of the grain size distributions (fig. 9), where the main source of sediment into the channel is restricted to seasonal inputs by ephemeral channels draining the surface of piedmont alluvial fans comprised of Upper Siwalik Group conglomerates (Kimura, 1999; Densmore and others, 2016). Hillslope processes are largely absent in these piedmont catchments where the primary source of sediment is from recycled Siwalik deposits, resulting in a much narrower input grain size distribution into the main Gandak channel. Subsurface D_{84} and D_{50} values measured on the Gandak within the Chitwan Dun vary by ~50 mm, compared to values of 100 to 200 mm upstream of the Dun (fig. 9).

In general, there is a strong correlation between subsurface and surface grain size measurements in terms of relative change between values down each profile. Whilst there is a clear surface coarsening visible, local changes in subsurface grain size are also reflected in surface grain size measurements, adding confidence to this sampling

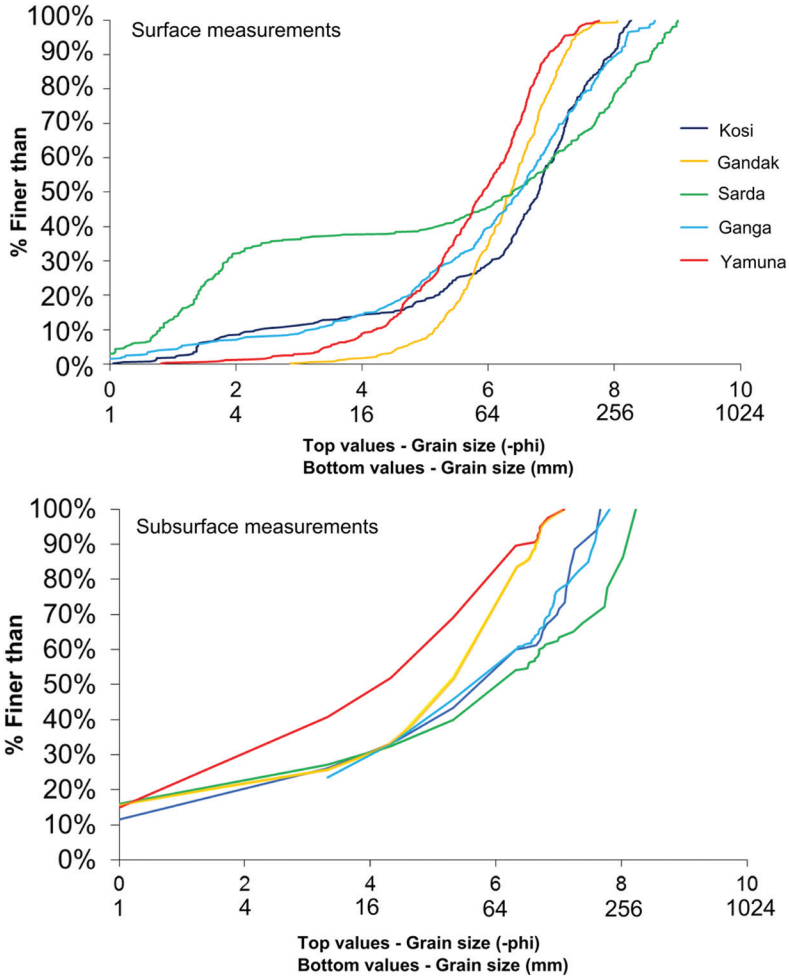

Fig. 8. Surface and subsurface grain size distributions of gravel bar sediment at the mountain outlet of each river.

approach. This trend is more apparent in the coarser (D_{84}) fraction of the sediment load (fig. 10). The position of the gravel-sand transition and downstream fining rates in each channel shows a considerable west to east variation (fig. 11), irrespective of the grain size distribution of the supplied sediment (fig. 8). The mapped position of the gravel-sand transition relative to the mountain front on each river suggests that gravel progrades further into the basin for rivers in the central and west Ganga Plain (fig. 11). For the Gandak and Kosi rivers in the east Ganga Plain, the gravel-sand transition was documented within 20 km downstream of the mountain front. The gravel-sand transition observed at the Yamuna, Ganga and Sharda rivers was notably further downstream at ~38, 28 and 45 km respectively. The gravel-sand transition was also not found to be an abrupt transition; in most instances a zone of ~2 to 5 km was noted where the bed was predominantly sand but large patches (up to 25% of the total bed fraction) of gravels were present, although these patches reduced in extent downstream. The position of the gravel-sand transition relative to long channel profiles (fig. 6) is

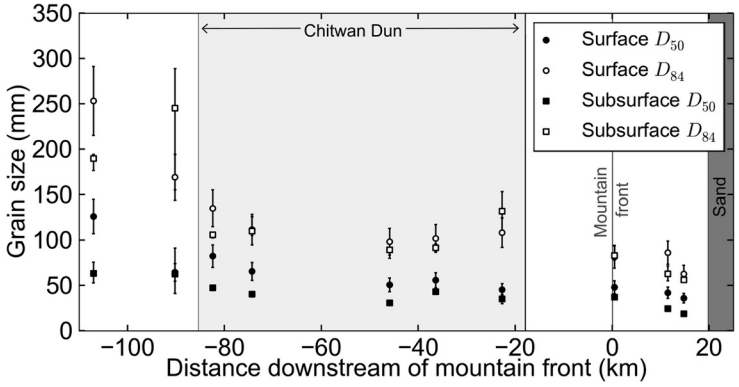

Fig. 9. D_{84} and D_{50} values along the Gandak River. A notable fining and overall narrowing of the grain size distribution is visible as the channel enters the Chitwan Dun, resulting in a much narrower grain size distribution being transported into the Ganga Plain.

coincident with a break in channel slope, where a steeper channel gradient exists upstream of the transition. This break in slope is less apparent in the east Ganga Plain on the Gandak and Kosi profiles, which may be explained by the noise in the DEM from which the long channel profiles were extracted. It seems more probable that any change in gradient associated with the gravel-sand transition is not as pronounced in the east Ganga Plain due to the gradients of these channels being lower overall. Upstream of the gravel-sand transition on the Sharda, Ganga and Yamuna, channel gradient and the absolute elevation of channels exiting the mountain front are also greater than for the Gandak and Kosi (fig. 12).

Fining rates were generally comparable across the Yamuna, Ganga and Sharda rivers (table 2 and fig. 13). For each site, r^2 values determined using each model were also near identical suggesting that the rate of exponential decay is very low (table 2). Using the linear decay model, fining rates of 1.31 to 4.75 mm/km were observed for D_{84} values across the Yamuna, Ganga, Sharda and Gandak channels whilst a rate of 10.5 mm/km was obtained for the Kosi (fig. 11). This same increase in fining rate is also apparent in the D_{50} fraction, where rates increase from 0.83 to 1.24 mm/km across systems in the west and central Plain, to 3.21 mm/km along the Kosi. Comparable spatial differences in fining exponents (α) obtained from the exponential model were

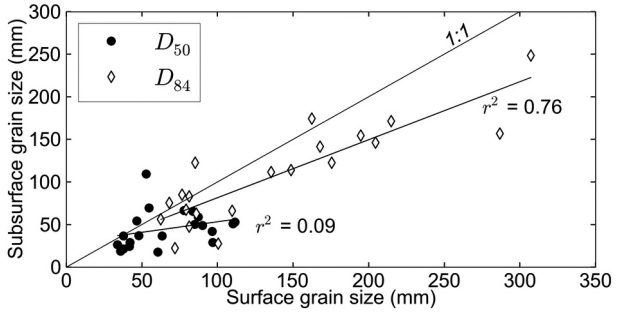

Fig. 10. Comparison of surface and subsurface measurements for the D_{84} (diamonds) and D_{50} (circles) values at each site across the Ganga Plain. There is a much stronger correlation between surface and subsurface values in the D_{84} values than D_{50}.

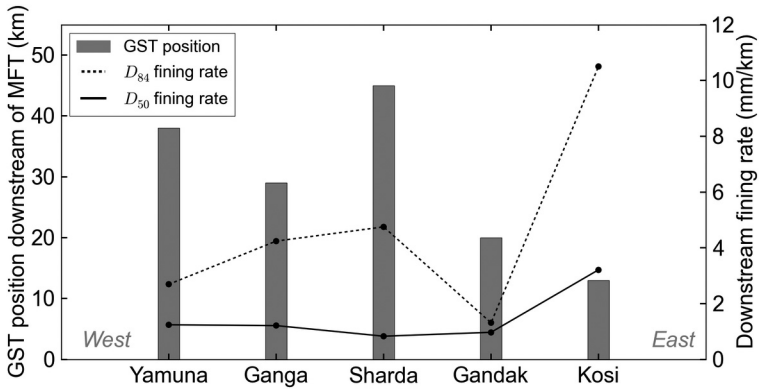

Fig. 11. Downstream distance from the mountain front (MFT) to the gravel-sand transition (GST) and linear model fining rates on averaged surface and subsurface D_{84} (dashed line) and D_{50} (solid line) grain sizes.

also found and are presented in figure 12. The relatively low fining exponent on the D_{84} fraction of the Gandak is likely to reflect upstream deposition of the coarsest fraction of the sediment load within the Chitwan Dun. As previously discussed, the grain size distribution exiting the Dun is much narrower (that is the D_{84} and D_{50} values are quite similar) on the Gandak relative to other systems (fig. 9). The D_{84} and D_{50} values are also lower than comparable sites at the mountain front in other systems.

DISCUSSION

Topographic analysis of the west Ganga Plain has highlighted the degree of channel entrenchment in the surface of the Yamuna and Ganga fans, compared to the relatively subdued surfaces of the Gandak and Kosi fans further east. Subsidence velocity estimates and downstream grain size fining rates have been found to be highest in the east Ganga Plain, where fan gradients are typically less steep and the gravel-sand transition is found closer to the mountain front. In the west Ganga Plain, the basement depth of the basin is notably lower than the east Ganga Plain, which when combined with known convergence velocities, suggests that the west Ganga Plain is subsiding less rapidly. Assuming basement gradient and convergence velocity yield a reasonable proxy for recent subsidence rates, then clear along strike variations in subsidence rate exist across the Ganga basin. These variations arise from differences in the elastic thickness of the underlying lithosphere (Lyon-Caen and Molnar, 1983, 1985; Jordan and Watts, 2005; Jackson and others, 2008) and/or local inherited morphological variations in the underthrust Indian basement (for example Lash, 1988) combined with varying convergent velocities. This is also consistent with published modeling results that have suggested the equivalent elastic thickness of the lithosphere is lower beneath the east Ganga Plain than the west (Jordan and Watts, 2005). This then raises the question of how, or whether, spatially variable subsidence can be expressed in the surface morphology of the Ganga Plain.

What Are the Timescales of the Controlling Processes?

Various modeling studies have suggested that the relative impact of increased and decreased subsidence rates, sediment flux, water supply and gravel fraction on basin stratigraphy/response is strongly dependent on the timescale over which these variations occur (for example Paola and others, 1992a; Heller and Paola, 1996; Duller and

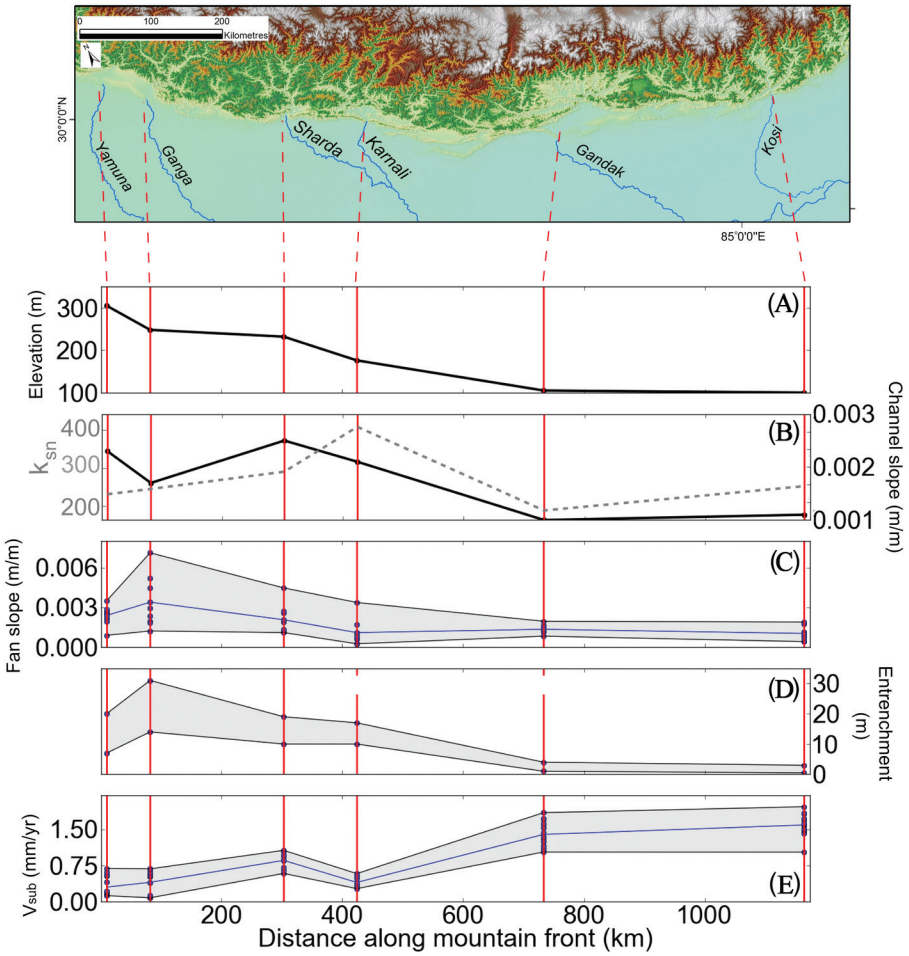

Fig. 12. Lateral variations in (A) outlet elevation, (B) 10 km average channel gradient and normalized channel steepness (k_{sn}) at fan apex and (C) proximal fan apex slopes, (D) channel entrenchment at the fan apex and (E) calculated subsidence velocity (V_{sub}) beneath the proximal foreland basin across the Ganga Plain.

others, 2010). To determine whether a forcing is slow or rapid, an equilibrium response time (T_{eq}) is calculated using the square of the basin length divided by the basin diffusivity (Paola and others, 1992a). For the Himalayan foreland basin, a T_{eq} of 2 Myr (±1 Myr) has been calculated (Heller and Paola, 1992). Variations in parameters that occur over a timescale lower than T_{eq} are subsequently termed as rapid, and those higher than T_{eq} as slow. Along strike of the orogen, variations in the position of the gravel-sand transition on the Yamuna, Ganga, Sharda, Gandak and Kosi rivers are consistent with long term (>1 Myr) patterns of subsidence across the basin where lower subsidence rates in the west result in a more distal gravel-sand transition than regions experiencing higher rates of subsidence in the east Ganga Plain, where a greater proportion of sediment is trapped in the proximal part of the basin due to a greater volume of accommodation being generated (Paola and others, 1992; Marr and others, 2000).

Table 2

D_{50} and D_{84} grain size fining rate data using both exponential and linear equations

	Exponential fit				***Linear fit***			
River	D_{84} α (km^{-1})	r^2	D_{50} α (km^{-1})	r^2	D_{84} β (mm/km)	r^2	D_{50} β (mm/km)	r^2
Yamuna	0.024	0.53	0.025	0.31	2.69	0.54	1.24	0.40
Ganga	0.032	0.81	0.022	0.20	4.24	0.80	1.21	0.15
Sharda	0.033	0.59	0.016	0.19	4.75	0.57	0.83	0.22
Gandak	0.019	0.52	0.031	0.36	1.31	0.50	0.97	0.38
Kosi	0.062	0.37	0.052	0.18	10.5	0.36	3.21	0.18

What Are the Spatial Characteristics of the Controlling Processes?

Previous works have also suggested that conditions imposed by local subsidence rates could modulate the gradient of large alluvial fan surfaces over millennial timescales (Allen P.A. and others, 2013). Longitudinal profiles of the Gandak, Sharda, Ganga and Yamuna rivers reveal a distinct break in slope at the gravel-sand transition (fig. 6). The transport coefficients of sand and gravel differ by a factor of ~10 (Marr and others, 2000) which, in combination with bed slope, determine the total flux of sediment at a point on the fluvial surface:

$$q_s(x,t) = -v\frac{\delta z(x,t)}{\delta x} \tag{8}$$

where q_s is sediment flux, v is the transport coefficient and z is the surface elevation. The transport coefficients of gravel and sand (v) are reported as 0.01 and 0.1 $km^2\,yr^{-1}$, respectively. These transport coefficient values incorporate a number of independently known or quantifiable variables including water discharge, Shields stress, dimensionless sediment flux and sediment porosity (Marr and others, 2000). At the gravel-sand transition, an increase in transport coefficient associated with a change from a gravel-bed to sand-bed river may occur; however, the associated reduction in channel slope would also be expected to reduce sediment flux along the profile. Analogue modeling of gravel bed channels has also suggested that a reduction in both total sediment flux and grain size, as a result of upstream deposition, will reduce the required transport capacity of the channel downstream. The progressively finer and smaller sediment load could therefore remain in transport within a channel with a lower gradient (Paola and others, 1992b). This is consistent with our observations across the Ganga Plain, where a relatively distinct change in channel slope is associated with the gravel-sand transition (fig. 5B). Interestingly, the positions of the gravel-sand transitions on the Gandak and Kosi rivers are directly comparable to those observed in smaller foothill or 'Piedmont' rivers (~8 – 20 km downstream of the mountain front). The catchment area of these Piedmont rivers ranges from ~25 to 350 km^2 (Dubille and Lavé, 2015) whilst the Gandak and Kosi catchment areas are an order of magnitude larger at ~31,000 km^2 and ~50,000 km^2, respectively (table 3). The gravel-sand transition on the Gandak, which lies ~100 km west of the foothill systems considered by Dubille and Lavé (2015), was noted at ~20 km. The transition on the Kosi, which lies ~100 km east of their study area, was noted at ~13 km. This suggests that the distance that gravel progrades out from the mountain front is not strongly dependent on upstream catchment area, and therefore unlikely to be dependent on absolute sediment flux, given the dramatically different catchment areas of the foothill and mountain catchments. However, the abrupt change in slope associated with the

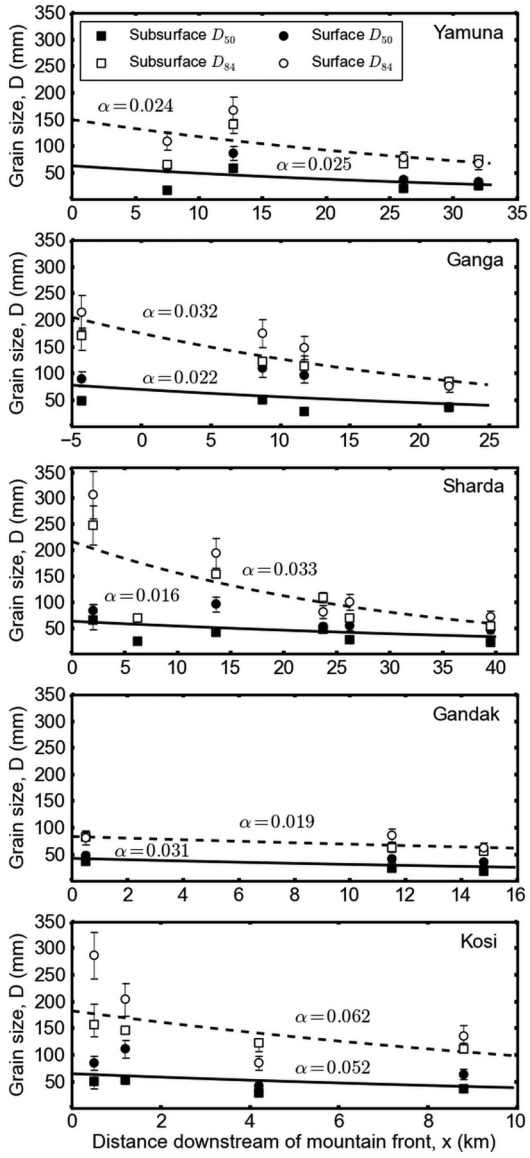

Fig. 13. Evolution of sediment grain size on gravel bars. Downstream fining exponents (α) for surface and subsurface averaged D_{84} and D_{50} values downstream of the mountain front for the Yamuna, Ganga, Sharda, Gandak and Kosi rivers. Error bars were calculated for surface samples by applying a ±15% error margin to account for subjective bias. Error margins on subsurface samples reflect the effects of the addition and removal of large clasts from the sample on D_{84} and D_{50} measurements. It should be noted that the scale of the horizontal axis is changing between plots.

gravel-sand transition is not a constant feature across these smaller Piedmont rivers. A less abrupt change in channel slope associated with the gravel-sand transition was observed in a number of smaller foothill-fed systems draining the Gandak-Kosi interfan area (Dubille and Lavé, 2015). In this instance, the subdued break in slope was attributed to the relative high proportion of sand relative to gravel transported by the

Table 3

Catchment and grain size sample summary information

	Catchment area (km^2)	Grain size sample location (UTM)			D_{84} (phi units)		D_{50} (phi units)		Distance downstream of MFT (km)	Slope (m/m)
					Surface	Subsurface	Surface	Subsurface		
Yamuna	9,419	43R	746512	3353763	6.78	6.05	5.92	4.15	7.5	0.00212
		43R	734615	3337112	7.39	7.14	6.45	5.88	12.7	0.00240
		43R	738113	3340361	6.31	6.08	5.24	4.41	26.1	0.00180
		43R	743686	3350341	6.09	6.24	5.08	4.72	32.0	0.00123
		43R	730761	3334533	GST	GST	GST	GST	38.1	0.00066
Ganga	19,666	44R	237430	3327606	7.75	7.42	6.49	5.62	-4.3	0.00177
		44R	226118	3311830	7.46	6.94	6.78	5.67	8.7	0.00192
		44R	226950	3308723	7.22	6.83	6.60	4.85	11.7	0.00189
		44R	227127	3298543	6.26	6.41	5.24	5.19	22.1	0.00122
		44R	228600	3293808	GST	GST	GST	GST	28.2	0.00084
Sharda	13.182	44R	416513	3219623	8.26	7.96	6.39	7.03	2	0.00252
		44R	414750	3216389	-	6.12	-	4.63	6.2	0.00237
		44R	412283	3210500	7.61	7.27	6.59	5.39	13.6	0.00191
		44R	413532	3201761	6.35	6.77	5.72	5.57	23.7	0.00170
		44R	413564	3199562	6.65	5.86	5.78	4.79	26.2	0.00161
		44R	413059	3187971	6.17	4.55	5.55	4.48	39.5	0.00068
		44R	414630	3183209	GST	GST	GST	GST	44.5	0.00040
Gandak	31,460	44R	790722	3041214	6.35	6.37	6.37	5.21	0	0.00134
		44R	782608	3035567	6.43	5.97	5.97	4.61	11.5	0.00080
		44R	781464	3032900	5.97	5.81	5.81	4.22	14.8	0.00079
		44R	782154	3028042	GST	GST	GST	GST	19.8	0.00020
Kosi	50,079	45R	514824	2969129	8.16	7.29	6.41	5.65	0	0.00031
		45R	514304	2968166	7.68	7.19	6.80	5.72	1.2	0.00030
		45R	515151	2965578	6.41	6.94	5.40	4.85	4.2	0.00029
		45R	512280	2962778	7.08	6.80	5.99	5.19	8.8	0.00126
		45R	511857	2958589	GST	GST	GST	GST	12.9	0.00057

channel at the mountain outlet, where a steep channel gradient was still needed to transport the large proportion of sand downstream of the transition. Where coarse gravels or conglomerate made up less than ~30 percent of the sediment load, no apparent break in slope was observed at the transition. Whether this same relationship scales up to the larger mountain fed systems has not been examined in detail.

The most dominant cause of a rapid reduction in grain size associated with the gravel-sand transition in aggrading systems has been attributed to selective sorting (for example Paola and others, 1992b; Ferguson and others, 1996), where downstream fining by selective sorting is enhanced by bedload sedimentation (Rice, 1999; Dubille and Lavé, 2015). Poorly sorted gravel mixtures and bimodal gravel inputs have been modeled to yield similar fining characteristics (Paola and others, 1992b), suggesting that rapid fining by selective deposition at the gravel-sand transition is insensitive to input sediment grain size distributions. Our current understanding of sediment flux to the Ganga basin is based on a synthesis of published fluxes calculated from ^{10}Be concentrations measured in modern river sediments (table 1). The variability within these data do not allow any robust conclusions to be drawn regarding spatial variations in the long-term sediment supply rate from the Himalayan catchments to the Ganga basin. A more thorough understanding in the observed variability in these ^{10}Be concentrations should be a target of future studies to better understand the role of sediment flux on these systems. Spatial variations in discharge from the Ganga catchment into the Plain could also contribute to the observed morphological signal. Whilst comparable discharge data are not available across these systems, the upstream catchment area of these systems yields an appropriate substitute, where numerous studies have shown a close correlation between these two variables (for example Knighton, 1998). In general, where larger catchment areas are observed in the east, larger discharges would also be expected (table 3) which is consistent with gauged measurements where available (Sinha and others, 2005). Annual precipitation estimates from the Tropical Rainfall Measuring Mission (TRMM) between 1998–2001 across the Himalaya have further suggested that precipitation is typically higher in catchments feeding into the east Ganga Plain (Anders and others, 2006). Interestingly, for a given sediment supply, increased rates of water supply have been modelled to correspond with advancing gravel fronts (Paola and others, 1992a). This doesn't appear to be a factor in the Ganga system where catchment area (and presumably discharge) are greatest in the east Ganga Plain, and the gravel-sand transition is found in its most proximal position. Given that it appears that the position of the gravel-sand transition is independent of variations in input grain size distributions, upstream catchment area and sediment flux, it is suggested that longer term patterns of subsidence rate are a governing control on the grain size transition in the modern Ganga Plain.

Where gravels prograde farthest downstream in the rivers of the central and west Ganga Plain, channel gradients are found to be steeper close to the mountain front. In the east Ganga Plain, lower channel gradients are observed upstream of the gravel-sand transition, where the relative change in channel gradient across the gravel-sand transition is also less pronounced. Channel gradient measurements derived from SRTM DEM elevations (fig. 6) are not of sufficient spatial resolution or quality to compare with grain size measurements obtained as part of this study. However, given the lack of obvious pattern in grain size distributions measured at the mountain front (fig. 8) and relatively subtle changes in channel gradient at the gravel-sand transition identified in the east Ganga Plain compared to the west (fig. 6), it seems improbable that differences in grain size can account for the along strike variations in channel gradient and grain size fining rates. Other possible interpretations of the variation in channel gradient are that profiles in the east experience higher subsidence rates at the

mountain front, resulting in the gravel-sand transition being closer to the mountain front. Late Holocene sedimentation rates of 0.62 to 1.45 mm/yr (Sinha and others, 1996) on the Ganga Plain are comparable or slightly lower than subsidence velocity estimates beneath the Kosi and Gandak Rivers of 1.6±0.6 and 1.4±0.4 mm/yr, respectively. Comparable information of sedimentation rates in the west Ganga Plain are not available. Alternatively, if there has been greater sediment flux in the west, then the channel may have experienced a greater degree of backfilling. Without evidence for the latter, we suggest higher differential subsidence in the east Ganga Plain as the most probable mechanism. Relative differences in fining exponents of the gravel fraction downstream of the mountain front are consistent with along strike variations in subsidence, where gravels in the Kosi River have a fining exponent two to three times greater than systems in the west Ganga Plain (fig. 13). Whilst the Gandak River has a relatively high subsidence velocity estimate, this same pattern in fining exponent is not as apparent and has been attributed to the buffering role of the upstream Chitwan Dun. Based on these observations, we interpret that spatial variations in subsidence rates play a controlling role in along strike variations in the longitudinal profiles of these rivers and grain size fining rates. However, spatially variable subsidence rates alone do not explain the entrenchment of the western rivers.

Climate and Signal Preservation

Top down changes in sediment and water discharges must have also influenced these systems (Sinha and others, 2005; Wobus and others, 2010). The seasonal nature of water and sediment delivery to the Ganga Plain is highly sensitive to variations in the strength of the Indian summer monsoon during which ~80 percent of the annual flow is discharged. From marine isotope stage 3 into the Last Glacial Maximum (LGM), a combination of low insolation and strong glacial conditions are thought to have significantly weakened the Indian summer monsoon and regional precipitation (Goodbred Jr., 2003; Gibling and others, 2005). This is also reflected in much lower runoff values interpreted from proxy records of palaeosalinity and $\delta^{18}O$ in the Bay of Bengal during the LGM (Cullen, 1981; Duplessy, 1982). Following the LGM, a variety of proxy records have suggested there was a widespread increase in precipitation, particularly after ~12 ka (Cullen, 1981; Goodbred Jr., 2003; Srivastava and others, 2003). How fluvial systems react to these climate driven variations in water and sediment discharges is more difficult to predict as both incision and aggradation can occur simultaneously within a catchment in response to a single perturbation (Tucker and Slingerland, 1997).

Numerous studies have examined the relationship between climatic transitions and phases of fluvial incision and aggradation (for example Tucker and Slingerland, 1997; Goodbred Jr., 2003; Gibling and others, 2005; Srivastava and others, 2008; Wobus and others, 2010; Duller and others, 2012; Densmore and others, 2016). Modeling results from Marr and others (2000) have suggested that a rapid increase (over timescales shorter than T_{eq}) in water flux and/or decrease in sediment flux can result in proximal erosion of gravel and advance of the gravel-sand transition. Rapid increases in sediment flux were also found to initiate an increase in proximal channel gradient and retreat of the gravel front (Marr and others, 2000). However, considerable variability in the geomorphic response generated by increased runoff intensity has also been modeled by Tucker and Slingerland (1997) using a physically based model of drainage basin evolution (GOLEM); significant variations in sediment flux were found to result from relatively modest variations in surface runoff, highlighting the difficulty in correlating a specific cause (climatic condition) to effect (geomorphic response). There are also complexities regarding how climatically driven waves of incision and aggradation are propagated downstream of the Himalaya into the Ganga Plain. The effects of stochastic forcing on sediment supply to channel networks has been

considered in previous studies (Benda and Dunne, 1997a, 1997b), where the intermittent storage and release of sediment within a catchment has been modeled to dramatically alter the sediment mass balance over thousand year time scales (Blöthe and Korup, 2013). Using both modeling outputs and circumstantial field evidence, unsteady sediment supply was found to affect channel morphology through the generation of sediment waves and transient phases of aggradation (Benda and Dunne, 1997b). If sediment transport through the catchment acts as a non-linear filter and buffers climatic signals (Jerolmack and Paola, 2010; Blöthe and Korup, 2013), it raises the question of what magnitude and wavelength of climatic forcing is capable of being recorded in the sedimentary record of the Ganga Plain?

Thermo-luminescence dating of quartz sands and radiocarbon dating on shell and calcrete materials preserved in the upper 2 to 8 m on the Ganga-Yamuna interfluve yield ages between 6 to 21 ka (summarized in Srivastava and others, 2003); these ages suggest that this was when the modern Ganga and Yamuna channels were last connected to the interfluve floodplain surface (Srivastava and others, 2003; Gibling and others, 2005). Such a situation is consistent with climatic fluctuations associated with the end of the LGM and subsequent strengthening of the Indian summer monsoon at ~11 to 7 ka (Goodbred Jr., 2003), which could have initiated widespread incision of channels into their respective mega-fans across the Ganga Plain. A corresponding increase in sediment delivery to the Bengal basin was also noted between ~11 to 7 ka, which translates to a mean sediment load of more than double current load estimates derived from late Holocene deposits in the basin (Goodbred and Kuehl, 2000). Estimates for sediment remobilisation during the early Holocene by incision across the Plain only account for ~2 to 25 percent of the total volume of sediment deposited into the basin during this period, suggesting that sediment flux exported from the Himalaya must have been considerably elevated (Goodbred Jr., 2003). Crucially, these observations in the Bengal basin imply that a wide scale climatic perturbation was rapidly propagated down the full length of the Ganga system. Whether this signal was locally amplified by reworking of vast deposits of stored sediment within the Himalaya (for example Blöthe and Korup, 2013) is unknown.

A downstream reduction in valley width and channel entrenchment identified on the Yamuna, Ganga and Karnali systems is consistent with a top down wave of incision, most likely initiated by a climate-induced increase in water or relative decrease in sediment discharges during the early Holocene (Tucker and Slingerland, 1997; Goodbred and Kuehl, 2000; Goodbred Jr., 2003; Wobus and others, 2010). However, this signal is not apparent in the east Ganga Plain where channels show minimal signs of entrenchment. Whilst some aggradation is thought to have occurred during the late Holocene, these rates are not thought to have been sufficient to infill earlier valley incision (Goodbred Jr., 2003). It therefore seems unlikely that the east Ganga Plain underwent any significant phase of incision, such as that experienced in the west Ganga Plain. This is consistent with well data drilled from the Kosi mega-fan (Singh and others, 1993) that suggested that the Kosi River has maintained a relatively mobile braided channel throughout the Holocene, which migrated across much of the surface of the mega-fan depositing a gravelly sand to fine sand unit.

Subsidence vs. Climate

The Kosi exhibits low channel and fan gradients, flows over the most rapidly subsiding portion of the basin and displays the highest sediment grain size fining rate. Where subsidence rates are higher, proximal vertical sedimentation rates would also be expected to be higher. This results in a smaller amount of sediment remaining in transport further downstream than for a comparable sediment flux in a system experiencing a slower rate of subsidence. The equilibrium gradient of the channel would therefore be expected to be lower where subsidence rates are higher and/or

where a greater proportion of the total sediment load is trapped in the proximal basin, as a channel with a lower gradient should be able to convey the smaller sediment load (Robinson and Slingerland, 1998). We hypothesize that patterns of incision and aggradation on this timescale reflect differences in the sensitivity of these systems to climatic forcing of sediment and water flux (Q_s and Q_w respectively), such as that experienced during the early Holocene in response to increased strength of the Indian summer monsoon between ~11 to 7 ka at the end of the LGM. The sensitivity of these systems to changes in Q_s and Q_w is dependent on the gradient of the equilibrium channel under the new Q_s and Q_w values relative to the subsidence controlled gradient of the wider fan surface, assuming that the channel was not originally entrenched. If the revised equilibrium channel gradient is lower than the original gradient of the alluvial fan, the channel will incise into the surface of the fan apex until a lower channel gradient is attained, producing an incised channel. For a constant climatic forcing of channel lowering along the strike of the Ganga Plain, incision will only occur where channel lowering rates outpace subsidence which will inherently be more difficult to achieve where subsidence rates are higher in the east Ganga Plain (fig. 14).

Based on upstream catchment areas and satellite-derived precipitation data, it seems likely that systems in the east Ganga Plain experience higher discharges than those further west. Discharge may play a key role in shaping the wider fan morphology, but the position of the modern gravel-sand transition is not consistent with these spatial variations in precipitation or possible variations in sediment flux, which could be related. Lower channel gradients in the east could reflect these higher water discharges (van den Berg, 1995; Knighton, 1998), but would fail to explain the triggering mechanism behind fan entrenchment in the west Ganga Plain. However, the proximal position of the gravel-sand transition and low channel gradients observed on the Kosi are consistent with the model results simulated under increased basin subsidence rates (over timescales greater than T_{eq}).

Whilst absolute sediment fluxes to the basins are uncertain, approximately 90 percent of the total flux is thought to bypass the basin (Lupker and others, 2011) which would suggest that sediment availability does not limit these systems. Again, the proximal position of the gravel-sand transition relative to the mountain front further suggests that the majority of this bypassed sediment is likely to be transported in suspension. Spatial variations in the amount of coarse bedload exported into the Plain, and deposited upstream of the gravel-sand transition, is unknown. Whilst beyond the scope of this study, this does appear to be a potential factor that could directly influence the morphology of these systems, as the entirety of this coarser sediment fraction is retained within the Plain. Further work is needed to better constrain the relative proportions of suspended load and bedload within the total sediment fluxes of these systems. The long term morphology of rivers in the east Ganga Plain appears to be primarily controlled by the relatively higher subsidence rates experienced in the eastern end of the basin. Furthermore, these systems appear to have been insensitive to wide scale changes in regional climate, such as that experienced at the end of the LGM, which initiated wide-spread incision in the west Ganga Plain.

CONCLUSIONS

A modified swath profile analysis has been applied to topographic data across much of the Himalayan foreland basin to characterize the broad nature of incision and aggradation over much of the Indo-Gangetic Plains. In general, we find that the degree of channel entrenchment increases from east to west across the Ganga Plain, and also decreases with distance downstream. First-order subsidence velocity estimates suggest a more rapidly subsiding basin in the east Ganga Plain with rates of up to 1.6 ± 0.6 mm/yr. Further west, subsidence velocity estimates decrease to as little as 0.3 ± 0.4

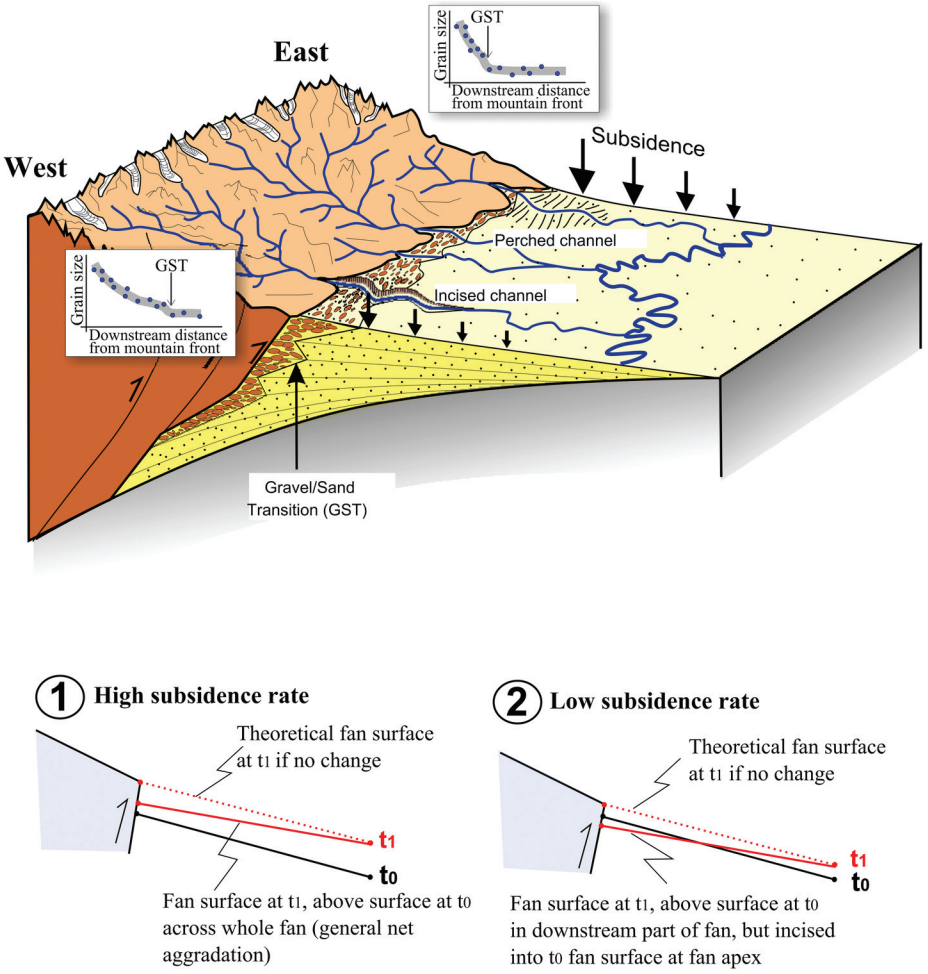

Fig. 14. Cartoon illustrating the role of variable subsidence rate on surface morphology across the Ganga Plain, in response to climate-driven variations in water and sediment discharge. The relative lowering of the surface between time steps t_0 (black line) and t_1 (red dashed line) is equivalent to a fall in base level, where the gradient of the fan surface is similar between surfaces. The rate of base level fall is controlled by subsidence in these scenarios where it is assumed invariant between the two time steps. A change in external forcing (sediment flux, discharge) leads to an adjustment (reduction in this instance) of the fan slope between t_0 and t_1 (red solid line), which can be accommodated with net aggradation where subsidence rates are high (1) but requires vertical incision into the fan apex where subsidence rates are lower (2).

mm/yr. Grain size fining rates are also found to closely reflect these patterns of subsidence, with the highest fining rates observed in the east Ganga Plain and lowest in the west. Furthermore, data currently available does not support a strong west to east variation in sediment flux at the thousand year timescale. Assuming that ~90 percent of sediment delivered into the foreland basin is bypassed downstream, it also seems more likely that the relative fraction of bedload delivered to the basin, which is trapped upstream of the gravel-sand transition, may have a more direct role on channel morphology than the total sediment flux. We propose that higher subsidence rates are responsible for a deeper basin in the east with perched, low gradient river channels that are relatively insensitive to climatically driven changes in base-level. In contrast,

the lower subsidence rates in the west are associated with a higher elevation basin topography, and entrenched river channels recording climatically induced lowering of river base-levels during the Holocene.

ACKNOWLEDGMENTS

We thank Ananta Gajurel, Jamie Stewart, Fred Bowyer, Konark Maheswari, Debojyoti Basuroy, Arkaprabha Sarkar, Bhairab Sitaula and Apex Adventure, and the Nepalese Department of Mines and Geology for their endless help, organisation and logistical support in the field. We are also grateful to the International Association of Sedimentologists, British Society for Geomorphology and the Edinburgh University Club of Toronto for their financial support of the fieldwork. Much of the motivation for this study originated from discussions with Prof. S. K. Tandon and Prof. R. Sinha while at a Royal Society/DST funded conference in Dehra Dun, India. This study formed part of a Natural Environment Research Council (NERC) funded Ph. D. (NE/L501566/1). We are grateful to reviewers Brian Dade and Paul Heller, and Associate Editor Sean Willett for valuable comments that helped modify the manuscript. Sadly, Paul Heller died unexpectedly before publication, and so this is likely to have been one of his last journal reviews. As a fervent advocate of integrating process sedimentology and basin analysis, and as someone with an ever-questioning mind, we would like to dedicate this contribution to his memory.

REFERENCES

Allen, G. H., Barnes, J. B., Pavelsky, T. M., and Kirby, E., 2013, Lithologic and tectonic controls on bedrock channel form at the northwest Himalayan front: Journal of Geophysical Research Earth Surface, v. 118, n. 3, p. 1806–1825, http://dx.doi.org/10.1002/jgrf.20113

Allen, P. A., and Allen, J. R., 2013, Basin Analysis: Principles and Application to Petroleum Play Assessment: West Sussex, England, John Wiley & Sons, 642 p.

Allen, P. A., Armitage, J. J., Carter, A., Duller, R. A., Michael, N. A., Sinclair, H. D., Whitchurch, A. L., and Whittaker, A. C., 2013, The Qs problem: Sediment volumetric balance of proximal foreland basin systems: Sedimentology, v. 60, n. 1, p. 102–130, http://dx.doi.org/10.1111/sed.12015

Amans, O., Beiping, W., and Ziggah, Y., 2013, Assessing vertical accuracy of SRTM Ver 4.1 and ASTER GDEM Ver 2 using differential GPS measurements- case study in Ondo State Nigeria: International Journal of Scientific & Engineering Research, v. 4, n. 12, p. 523–531.

Andermann, C., Crave, A., Gloaguen, R., Davy, P., and Bonnet, S., 2012, Connecting source and transport: Suspended sediments in the Nepal Himalayas: Earth and Planetary Science Letters, v. 351–352, p.158–170, http://dx.doi.org/10.1016/j.epsl.2012.06.059

Anders, A. M., Roe, G. H., Hallet, B., Montgomery, D. R., Finnegan, N. J., and Putkonen, J., 2006, Spatial patterns of precipitation and topography in the Himalaya: Geological Society of America Special Paper, v. 398, p. 39–53, http://dx.doi.org/10.1130/2006.2398(03)

Attal, M., and Lavé, J., 2006, Changes of bedload characteristics along the Marsyandi River (central Nepal): Implications for understanding hillslope sediment supply, sediment load evolution along fluvial networks, and denudation in active orogenic belts, *in* Tectonics, Climate and Landscape Evolution: Geological Society of America Special Paper, v. 398, p. 143–171, http://dx.doi.org/10.1130/2006.2398(09)

Attal, M., Mudd, S. M., Hurst, M. D., Weinman, B., Yoo, K., and Naylor, M., 2015, Impact of change in erosion rate and landscape steepness on hillslope and fluvial sediments grain size in the Feather River basin (Sierra Nevada, California): Earth Surface Dynamics, v. 3, p. 201–222, http://dx.doi.org/10.5194/esurf-3-201-2015

Benda, L., and Dunne, T., 1997a, Stochastic forcing of sediment supply to channel networks from landsliding and debris flow: Water Resources Research, v. 33, n. 12, p. 2849–2863, http://dx.doi.org/10.1029/97WR02388

——— 1997b, Stochastic forcing of sediment routing and storage in channel networks: Water Resources Research, v. 33, n. 12, p. 2865–2880, http://dx.doi.org/10.1029/97WR02387

Blöthe, J. H., and Korup, O., 2013, Millennial lag times in the Himalayan sediment routing system: Earth and Planetary Science Letters, v. 382, p. 38–46, http://dx.doi.org/10.1016/j.epsl.2013.08.044

Bookhagen, B., and Burbank, D. W., 2006, Topography, relief, and TRMM-derived rainfall variations along the Himalaya: Geophysical Research Letters, v. 33, n. 8, L08405, http://dx.doi.org/10.1029/2006GL026037

Bookhagen, B., Thiede, R. C., and Strecker, M. R., 2005, Abnormal monsoon years and their control on erosion and sediment flux in the high, arid northwest Himalaya: Earth and Planetary Science Letters, v. 231, p. 131–146, http://dx.doi.org/10.1016/j.epsl.2004.11.014

Bridge, J. S., and Leeder, M. R., 1979, A simulation model of alluvial stratigraphy: Sedimentology, v. 26, n. 5, p. 617–644, http://dx.doi.org/10.1111/j.1365-3091.1979.tb00935.x
Brozovic, N., and Burbank, D. W., 2000, Dynamic fluvial systems and gravel progradation in the Himalayan foreland: Geological Society of America Bulletin, v. 112, n. 3, p. 394–412, http://dx.doi.org/10.1130/0016-7606(2000)112<394:DFSAGP>2.0.CO;2
Bryant, M., Falk, P., and Paola, C., 1995, Experimental study of avulsion frequency and rate of deposition: Geology, v. 23, n. 4, p. 365–368, http://dx.doi.org/10.1130/0091-7613(1995)023<0365:ESOAFA>2.3.CO;2
Burbank, D. W., 1992, Causes of recent Himalayan uplift deduced from deposited patterns in the Ganges basin: Nature, v. 357, p. 680–683, http://dx.doi.org/10.1038/357680a0
Burbank, D. W., and Beck, R. A., 1991, Models of aggradation versus progradation in the Himalayan Foreland: Geologische Rundschau, v. 80, n. 3, p. 623–638, http://dx.doi.org/10.1007/BF01803690
Burbank, D. W., Beck, R. A., and Mulder, T., 1996, The Himalayan foreland basin, *in* Yin, A., and Harrison, editors, The Tectonic Evolution of Asia: Cambridge, England, Cambridge University Press, p. 149–188.
Chakraborty, T., and Ghosh, P., 2010, The geomorphology and sedimentology of the Tista megafan, Darjeeling Himalaya: Implications for megafan building processes: Geomorphology, v. 115, n. 3–4, p. 252–266, http://dx.doi.org/10.1016/j.geomorph.2009.06.035
Chakraborty, T., Kar, R., Ghosh, P., and Basu, S., 2010, Kosi megafan: Historical records, geomorphology and the recent avulsion of the Kosi River: Quaternary International, v. 227, n. 2, p. 143–160, http://dx.doi.org/10.1016/j.quaint.2009.12.002
Church, M. A., McLean, D. G., and Wolcott, J. F., 1987, River bed gravels: Sampling and analysis, *in* Thorne, C. R., Bathurst, J. C., and Hey, R. D., editors, Sediment Transport in Gravel-Bed Rivers: New York, John Wiley and Sons New York, p. 43–88.
Cullen, J. L., 1981, Microfossil evidence for changing salinity patterns in the Bay of Bengal over the last 20 000 years: Palaeogeography, Palaeoclimatology, Palaeoecology, v. 35, p. 315–356, http://dx.doi.org/10.1016/0031-0182(81)90101-2
Dade, W. B., 2000, Grain size, sediment transport and alluvial channel pattern: Geomorphology, v. 35, n. 1–2, p. 119–126, http://dx.doi.org/10.1016/S0169-555X(00)00030-1
Dade, W. B., and Friend, P. F., 1998, Grain–Size, Sediment–Transport Regime, and Channel Slope in Alluvial Rivers: The Journal of Geology, v. 106, p. 661–676, http://dx.doi.org/10.1086/516052
DeCelles, P. G., and Giles, K. A., 1996, Foreland basin systems: Basin Research, v. 8, n. 2, p. 105–123, http://dx.doi.org/10.1046/j.1365-2117.1996.01491.x
Densmore, A. L., Sinha, R., Sinha, S., Tandon, S. K., and Jain, V., 2016, Sediment storage and release from Himalayan piggyback basins and implications for downstream river morphology and evolution: Basin Research, v. 28, n. 4, p. 1–16, http://dx.doi.org/10.1111/bre.12116
Dietrich, W. E., Kirchner, J. W., Ikeda, H., and Iseya, F., 1989, Sediment supply and the development of the coarse surface layer in gravel-bedded rivers: Nature, v. 340, p. 215–217, http://dx.doi.org/10.1038/340215a0
Dubille, M., and Lavé, J., 2015, Rapid grain size coarsening at sandstone / conglomerate transition: Similar expression in Himalayan modern rivers and Pliocene molasse deposits: Basin Research, v. 27, n. 1, p. 26–42, http://dx.doi.org/10.1111/bre.12071
Duller, R. A., Whittaker, A. C., Fedele, J. J., Whitchurch, A. L., Springett, J., Smithells, R., Fordyce, S., and Allen, P. A., 2010, From grain size to tectonics: Journal of Geophysical Research Earth Surface, v. 115, F03022, http://dx.doi.org/10.1029/2009JF001495
Duller, R. A., Whittaker, A. C., Swinehart, J. B., Armitage, J. J., Sinclair, H. D., Bair, A., and Allen, P. A., 2012, Abrupt landscape change post–6 Ma on the central Great Plains, USA: Geology, v. 40, n. 10, p. 871–874, http://dx.doi.org/10.1130/G32919.1
Duplessy, J. C., 1982, Glacial to interglacial contrasts in the northern Indian Ocean: Nature, v. 295, p. 494–498, http://dx.doi.org/10.1038/295494a0
Fedele, J. J., and Paola, C., 2007, Similarity solutions for fluvial sediment fining by selective deposition: Journal of Geophysical Research Earth Surface, v. 112, n. F2, http://dx.doi.org/10.1029/2005JF000409
Feldl, N., and Bilham, R., 2006, Great Himalayan earthquakes and the Tibetan plateau: Nature, v. 444, p. 165–170, http://dx.doi.org/10.1038/nature05199
Ferguson, R., Hoey, T., Wathen, S., and Werritty, A., 1996, Field evidence for rapid downstream fining of river gravels through selective transport: Geology, v. 24, n. 2, p. 179–182, http://dx.doi.org/10.1130/0091-7613(1996)024<0179:FEFRDF>2.3.CO;2
Fleitmann, D., Burns, S. J., Mangini, A., Mudelsee, M., Kramers, J., Villa, I., Neff, U., Al-Subbary, A. A., Buettner, A., Hippler, D., and Matter, A., 2007, Holocene ITCZ and Indian monsoon dynamics recorded in stalagmites from Oman and Yemen (Socotra): Quaternary Science Reviews, v. 26, n. 1–2, p. 170–188, http://dx.doi.org/10.1016/j.quascirev.2006.04.012
Flemings, P. B., and Jordan, T. E., 1989, A synthetic stratigraphic model of foreland basin development: Journal of Geophysical Research Solid Earth, v. 94, n. B4, p. 3851–3866, http://dx.doi.org/10.1029/JB094iB04p03851
Ghimire, G. P. S., and Uprety, B. K., 1990, Causes and effects of siltation on the environment of Nepal: Environmentalist, v. 10, n. 1, p. 55–65, http://dx.doi.org/10.1007/BF02239558
Gibling, M. R., Tandon, S. K., Sinha, R., and Jain, M., 2005, Discontinuity-Bounded Alluvial Sequences of the Southern Gangetic Plains, India: Aggradation and Degradation in Response to Monsoonal Strength: Journal of Sedimentary Research, v. 75, n. 3, p. 369–385, http://dx.doi.org/10.2110/jsr.2005.029
Godard, V., Bourlès, D. L., Spinabella, F., Burbank, D. W., Bookhagen, B., Fisher, G. B., Moulin, A., and Léanni, L., 2014, Dominance of tectonics over climate in Himalayan denudation: Geology, v. 42, n. 3, p. 243–246, G35342.1, http://dx.doi.org/10.1130/G35342.1
Goodbred, S. L., Jr., 2003, Response of the Ganges dispersal system to climate change: A source-to-sink view

since the last interstade: Sedimentary Geology, v. 162, n. 1–2, p. 83–104, http://dx.doi.org/10.1016/S0037-0738(03)00217-3
Goodbred, S. L., Jr., and Kuehl, S. A., 2000, Enormous Ganges-Brahmaputra sediment discharge during strengthened early Holocene monsoon: Geology, v. 28, n. 12, p. 1083–1086, http://dx.doi.org/10.1130/0091-7613(2000)28<1083:EGSDDS>2.0.CO;2
Heller, P. L., and Paola, C., 1992, The large-scale dynamics of grain-size variation in alluvial basins, 2: Application to syntectonic conglomerate: Basin Research, v. 4, n. 2, p. 91–102, http://dx.doi.org/10.1111/j.1365-2117.1992.tb00146.x
——— 1996, Downstream Changes In Alluvial Architecture: An Exploration of Controls on Channel-stacking Patterns: Journal of Sedimentary Research, v. 66, n. 2, p. 297–306, http://dx.doi.org/10.1306/D4268333-2B26-11D7-8648000102C1865D
Hergarten, S., Robl, J., and Stüwe, K., 2014, Extracting topographic swath profiles across curved geomorphic features: Earth Surface Dynamics, v. 2, p. 97–104, http://dx.doi.org/10.5194/esurf-2-97-2014
Hoth, S., Hoffmann-Rothe, A., and Kukowski, N., 2007, Frontal accretion: An internal clock for bivergent wedge deformation and surface uplift: Journal of Geophysical Research Solid Earth, v. 112, n. B6, http://dx.doi.org/10.1029/2006JB004357
Immerzeel, W. W., van Beek, L. P. H., and Bierkens, M. F. P., 2010, Climate Change Will Affect the Asian Water Towers: Science, v. 328, n. 5984, p. 1382–1385, http://dx.doi.org/10.1126/science.1183188
Jackson, J., McKenzie, D., Priestley, K., and Emmerson, B., 2008, New views on the structure and rheology of the lithosphere: Journal of the Geological Society, v. 165, n. 2, p. 453–465, http://dx.doi.org/10.1144/0016-76492007-109
Jain, V., and Sinha, R., 2003, River systems in the Gangetic plains and their comparison with the Siwaliks: A review: Current Science, v. 84, n. 8, p. 1025–1033.
Jerolmack, D. J., and Paola, C., 2010, Shredding of environmental signals by sediment transport: Geophysical Research Letters, v. 37, n. 19, L19401, http://dx.doi.org/10.1029/2010GL044638
Jha, P. K., Vaithiyanathan, P., and Subramanian, V., 1993, Mineralogical characteristics of the sediments of a Himalayan river: Yamuna River– a tributary of the Ganges: Environmental Geology, v. 22, n. 1, p. 13–20, http://dx.doi.org/10.1007/BF00775279
Jordan, T. A., and Watts, A. B., 2005, Gravity anomalies, flexure and the elastic thickness structure of the India–Eurasia collisional system: Earth and Planetary Science Letters, v. 236, n. 3–4, p. 732–750, http://dx.doi.org/10.1016/j.epsl.2005.05.036
Kellerhals, R., and Bray, D. I., 1971, Sampling procedures for coarse fluvial sediments: Journal of Hydraulic Engineering, v. 97, p. 1165–1180.
Kimura, K., 1999, Diachronous evolution of sub-Himalayan piggyback basins, Nepal: Island Arc, v. 8, n. 1, p. 99–113, http://dx.doi.org/10.1046/j.1440-1738.1999.00224.x
Knighton, D., 1998, Fluvial Forms and Processes: A New Perspective, London, Routledge, 383 p.
Kumar, R., Sangode, S. J., and Ghosh, S. K., 2004, A multistorey sandstone complex in the Himalayan Foreland Basin, NW Himalaya, India: Journal of Asian Earth Sciences, v. 23, n. 3, p. 407–426, http://dx.doi.org/10.1016/S1367-9120(03)00176-7
Lash, G. G., 1988, Along-strike variations in foreland basin evolution: Possible evidence for continental collision along an irregular margin: Basin Research, v. 1, n. 2, p. 71–83, http://dx.doi.org/10.1111/j.1365-2117.1988.tb00006.x
Lavé, J., and Avouac, J. P., 2000, Active folding of fluvial terraces across the Siwalik Hills, Himalayas of central Nepal: Journal of Geophysical Research Solid Earth, v. 105, n. B3, p. 5735–5770, http://dx.doi.org/10.1029/1999JB900292
——— 2001, Fluvial incision and tectonic uplift across the Himalayas of central Nepal: Journal of Geophysical Research Solid Earth, v. 106, n. B11, p. 26561–26591, http://dx.doi.org/10.1029/2001JB000359
Leeder, M. R., Harris, T., and Kirkby, M. J., 1998, Sediment supply and climate change: Implications for basin stratigraphy: Basin Research, v. 10, n. 1, p. 7–18, http://dx.doi.org/10.1046/j.1365-2117.1998.00054.x
Lupker, M., France-Lanord, C., Lavé, J., Bouchez, J., Galy, V., Métivier, F., Gaillardet, J., Lartiges, B., and Mugnier, J.-L., 2011, A Rouse-based method to integrate the chemical composition of river sediments: Application to the Ganga basin. Journal of Geophysical Research Earth Surface, v. 116, n. F4, http://dx.doi.org/10.1029/2010JF001947
Lupker, M., Blard, P.-H., Lavé, J., France-Lanord, C., Léanni, L., Puchol, N., Charreau, J., and Bourlès, D., 2012, ^{10}Be-derived Himalayan denudation rates and sediment budgets in the Ganga basin: Earth and Planetary Science Letters, v. 333–334, p. 146–156, http://dx.doi.org/10.1016/j.epsl.2012.04.020
Lyon-Caen, H., and Molnar, P., 1983, Constraints on the structure of the Himalaya from an analysis of gravity anomalies and a flexural model of the lithosphere: Journal of Geophysical Research Solid Earth, v. 88, n. B10, p. 8171–8191, http://dx.doi.org/10.1029/JB088iB10p08171
——— 1985, Gravity anomalies, flexure of the Indian Plate, and the structure, support and evolution of the Himalaya and Ganga Basin: Tectonics, v. 4, n. 6, p. 513–538, http://dx.doi.org/10.1029/TC004i006p00513
Marr, J. G., Swenson, J. B., Paola, C., and Voller, V. R., 2000, A two-diffusion model of fluvial stratigraphy in closed depositional basins: Basin Research, v. 12, n. 3–4, p. 381–398, http://dx.doi.org/10.1046/j.1365-2117.2000.00134.x
Mugnier, J.-L., and Huyghe, P., 2006, Ganges basin geometry records a pre-15 Ma isostatic rebound of Himalaya: Geology, v. 34, n. 6, p. 445–448, http://dx.doi.org/10.1130/G22089.1
Mugnier, J. L., Leturmy, P., Mascle, G., Huyghe, P., Chalaron, E., Vidal, G., Husson, L., and Delcaillau, B., 1999, The Siwaliks of western Nepal: I. Geometry and kinematics: Journal of Asian Earth Sciences, v. 17, n. 5–6, p. 629–642, http://dx.doi.org/10.1016/S1367-9120(99)00038-3

Narula, P. L., Acharyya, S. K., and Banerjee, J., 2000, Seismotectonic Atlas of India and its Environs: Calcutta, India, The Geological Survey of India.
Naylor, M., and Sinclair, H. D., 2007, Punctuated thrust deformation in the context of doubly vergent thrust wedges: Implications for the localization of uplift and exhumation: Geology, v. 35, n. 6, p. 559–562, http://dx.doi.org/10.1130/G23448A.1
Paola, C., and Seal, R., 1995, Grain Size Patchiness as a Cause of Selective Deposition and Downstream Fining: Water Resources Research, v. 31, n. 5, p. 1395–1407, http://dx.doi.org/10.1029/94WR02975
Paola, C., Heller, P. L., and Angevine, C. L., 1992a, The large-scale dynamics of grain-size variation in alluvial basins, 1: Theory: Basin Research, v. 4, n. 2, p. 73–90, http://dx.doi.org/10.1111/j.1365-2117.1992.tb00145.x
Paola, C., Parker, G., Seal, R., Sinha, S. K., Southard, J. B., and Wilcock, P. R., 1992b, Downstream Fining by Selective Deposition in a Laboratory Flume: Science, v. 258, n. 5089, p. 1757–1760, http://dx.doi.org/10.1126/science.258.5089.1757
Parker, G., 1990, Surface-based bedload transport relation for gravel rivers: Journal of Hydraulic Research, v. 28, n. 4, p. 417–436, http://dx.doi.org/10.1080/00221689009499058
Parker, G., and Toro-Escobar, C. M., 2002, Equal mobility of gravel in streams: The remains of the day: Water Resources Research, v. 38, n. 11, p. 46-1–46-8, http://dx.doi.org/10.1029/2001WR000669
Rice, S., 1999, The Nature and Controls on Downstream Fining Within Sedimentary Links: Journal of Sedimentary Research, v. 69, n. 1, p. 32–39, http://dx.doi.org/10.2110/jsr.69.32
Rice, S. P., and Church, M., 2001, Longitudinal profiles in simple alluvial systems: Water Resources Research, v. 37, n. 2, p. 417–426, http://dx.doi.org/10.1029/2000WR900266
Robinson, R. A. J., and Slingerland, R. L., 1998, Origin of Fluvial Grain-Size Trends in a Foreland Basin: The Pocono Formation on the Central Appalachian Basin: Journal of Sedimentary Research, v. 68, n. 3, p. 473–486, http://dx.doi.org/10.2110/jsr.68.473
Shah, B. A., 2007, Role of Quaternary stratigraphy on arsenic-contaminated groundwater from parts of Middle Ganga Plain, UP–Bihar, India: Environmental Geology, v. 53, n. 7, p. 1553–1561, http://dx.doi.org/10.1007/s00254-007-0766-y
Shukla, U. K., Singh, I. B., Sharma, M., and Sharma, S., 2001, A model of alluvial megafan sedimentation: Ganga Megafan: Sedimentary Geology, v. 44, n. 3–4, p. 243–262. http://dx.doi.org/10.1016/S0037-0738(01)00060-4
Shukla, U. K., Srivastava, P., and Singh, I. B., 2012, Migration of the Ganga River and development of cliffs in the Varanasi region, India during the late Quaternary: Role of active tectonics: Geomorphology, v. 171–172, p. 101–113, http://dx.doi.org/10.1016/j.geomorph.2012.05.009
Sinclair, H. D., and Naylor, M., 2012, Foreland basin subsidence driven by topographic growth versus plate subduction: Geological Society of America Bulletin, v. 124, n. 3, p. 368–379, http://dx.doi.org/10.1130/b30383.1
Singh, H., Parkash, B., and Gohain, K., 1993, Facies analysis of the Kosi megafan deposits: Sedimentary Geology, v. 85, n. 1–4, p. 87–113, http://dx.doi.org/10.1016/0037-0738(93)90077-I
Singh, I. B., 1996, Geological evolution of Ganga Plain - an overview: Journal of the Palaeontological Society of India, v. 41, p. 99–137.
Sinha, R., 2005, Why do Gangetic rivers aggrade or degrade?: Current Science, v. 89, n. 5, p. 836–840.
Sinha, R., and Friend, P. F., 1994, River systems and their sediment flux, Indo-Gangetic plains, Northern Bihar, India: Sedimentology, v. 41, n. 4, p. 825–845, http://dx.doi.org/10.1111/j.1365-3091.1994.tb01426.x
Sinha, R., Friend, P. F., and Switsur, V. R., 1996, Radiocarbon dating and sedimentation rates in the Holocene alluvial sediments of the northern Bihar plains, India: Geological Magazine London, v. 133, n. 1, p. 85–90, http://dx.doi.org/10.1017/S0016756800007263
Sinha, R., Jain, V., Babu, G. P., and Ghosh, S., 2005, Geomorphic characterization and diversity of the fluvial systems of the Gangetic Plains: Geomorphology, v. 70, n. 3–4, p. 207–225, http://dx.doi.org/10.1016/j.geomorph.2005.02.006
Sinha, R., Kettanah, Y., Gibling, M. R., Tandon, S. K., Jain, M., Bhattacharjee, P. S., Dasgupta, A. S., and Ghazanfari, P., 2009, Craton-derived alluvium as a major sediment source in the Himalayan Foreland Basin of India: Geological Society of America Bulletin, v. 121, n. 1112, p. 1596–1610, http://dx.doi.org/10.1130/B26431.1
Sinha, R., Gaurav, K., Chandra, S., and Tandon, S. K., 2013, Exploring the channel connectivity structure of the August 2008 avulsion belt of the Kosi River, India: Application to flood risk assessment: Geology, v. 41, n. 10, p. 1099–1102, http://dx.doi.org/10.1130/G34539.1
Sinha, R., Sripriyanka, K., Jain, V., and Mukul, M., 2014a, Avulsion threshold and planform dynamics of the Kosi River in north Bihar (India) and Nepal: A GIS framework: Geomorphology, v. 216, p. 157–170, http://dx.doi.org/10.1016/j.geomorph.2014.03.035
Sinha, R., Ahmad, J., Gaurav, K., and Morin, G., 2014b, Shallow subsurface stratigraphy and alluvial architecture of the Kosi and Gandak megafans in the Himalayan foreland basin, India: Sedimentary Geology, v. 301, p. 133–149, http://dx.doi.org/10.1016/j.sedgeo.2013.06.008
Slingerland, R., and Smith, N. D., 2004, River Avulsions and Their Deposits: Annual Review of Earth and Planetary Sciences, v. 32, p. 257–285, http://dx.doi.org/10.1146/annurev.earth.32.101802.120201
Srivastava, P., Singh, I. B., Sharma, M., and Singhvi, A. K., 2003, Luminescence chronometry and Late Quaternary geomorphic history of the Ganga Plain, India, *in* Gupta, A. K., Anderson, D. M., and Malmgren, B. A., editors, Indian Ocean Monsoons: Land and Sea Record: Palaeogeography, Palaeoclimatology, Palaeoecology, v. 197, n. 1–2, p. 15–41, http://dx.doi.org/10.1016/S0031-0182(03)00384-5
Srivastava, P., Tripathi, J. K., Islam, R., and Jaiswal, M. K., 2008, Fashion and phases of late Pleistocene aggradation and incision in the Alaknanda River Valley, western Himalaya, India: Quaternary Research, v. 70, n. 1, p. 68–80, http://dx.doi.org/10.1016/j.yqres.2008.03.009

Sternberg, H., 1875, Untersuchungen über längen-und querprofil geschiebeführender flüsse: Zeitschrift für Bauwesen, v. 25, p. 483–506.
Stevens, V. L., and Avouac, J. P., 2015, Interseismic coupling on the main Himalayan thrust: Geophysical Research Letters, v. 42, n. 14, p. 5828–5837, http://dx.doi.org/10.1002/2015GL064845
Syvitski, J. P. M., and Brakenridge, G. R., 2013, Causation and avoidance of catastrophic flooding along the Indus River, Pakistan: GSA Today, v. 23, p. 4–10, http://dx.doi.org/10.1130/GSATG165A.1
Tandon, S. K., Gibling, M. R., Sinha, R., Singh, V., Ghazanfari, P., Dasgupta, A., Jain, M., and Jain, V., 2006, Alluvial Valleys of the Ganga Plains, India: Timing and Causes of Incision, *in* Dalrymple, R. W., Leckie, D. A., and Tilliman, R. W., editors, Incised Valleys in Time and Space: SEPM Special Publication, v. 85, p. 15–35, http://dx.doi.org/10.2110/pec.06.85.0015
Telbisz, T., Kovács, G., Székely, B., and Szabó, J., 2013, Topographic swath profile analysis: A generalization and sensitivity evaluation of a digital terrain analysis tool: Zeitschrift für Geomorphologie, v. 57, n. 4, p. 485–513, http://dx.doi.org/10.1127/0372-8854/2013/0110
Thiede, R. C., and Ehlers, T. A., 2013, Large spatial and temporal variations in Himalayan denudation: Earth and Planetary Science Letters, v. 371–372, p. 278–293, http://dx.doi.org/10.1016/j.epsl.2013.03.004
Tucker, G. E., and Slingerland, R., 1997, Drainage basin responses to climate change: Water Resources Research, v. 33, n. 8, p. 2031–2047, http://dx.doi.org/10.1029/97WR00409
van den Berg, J. H., 1995, Prediction of alluvial channel pattern of perennial rivers: Geomorphology, v. 12, n. 4, p. 259–279, http://dx.doi.org/10.1016/0169-555X(95)00014-V
Vance, D., Bickle, M., Ivy-Ochs, S., and Kubik, P. W., 2003, Erosion and exhumation in the Himalaya from cosmogenic isotope inventories of river sediments: Earth and Planetary Science Letters, v. 206, n. 3–4, p. 273–288, http://dx.doi.org/10.1016/S0012-821X(02)01102-0
Wasson, R. J., 2003, A sediment budget for the Ganga-Brahmaputra catchment: Current Science, v. 84, n. 8, p. 1041–1047.
Wells, N. A., and Dorr, J. A., 1987, Shifting of the Kosi River, northern India: Geology, v. 15, n. 3, p. 204–207, http://dx.doi.org/10.1130/0091-7613(1987)15<204:SOTKRN>2.0.CO;2
Wesnousky, S. G., Kumar, S., Mohindra, R., and Thakur, V. C., 1999, Uplift and convergence along the Himalayan Frontal Thrust of India: Tectonics, v. 18, n. 6, p. 967–976, http://dx.doi.org/10.1029/1999TC900026
Whittaker, A. C., Attal, M., and Allen, P. A., 2010, Characterising the origin, nature and fate of sediment exported from catchments perturbed by active tectonics: Basin Research, v. 22, n. 6, p. 809–828, http://dx.doi.org/10.1111/j.1365-2117.2009.00447.x
Whittaker, A. C., Duller, R. A., Springett, J., Smithells, R. A., Whitchurch, A. L., and Allen, P. A., 2011, Decoding downstream trends in stratigraphic grain size as a function of tectonic subsidence and sediment supply: Geological Society of America Bulletin, v. 123, p. 1363–1382, http://dx.doi.org/10.1130/B30351.1
Wobus, C., Whipple, K. X., Kirby, E., Snyder, N., Johnson, J., Spyropolou, K., Crosby, B., and Sheehan, D., 2006, Tectonics from topography: Procedures, promise, and pitfalls: Geological Society of America Special Papers, v. 398, p. 55–74, http://dx.doi.org/10.1130/2006.2398(04)
Wobus, C. W., Tucker, G. E., and Anderson, R. S., 2010, Does climate change create distinctive patterns of landscape incision?: Journal of Geophysical Research Earth Surface, v. 115, n. F4, , http://dx.doi.org/10.1029/2009JF001562
Yin, A., 2006, Cenozoic tectonic evolution of the Himalayan orogen as constrained by along-strike variation of structural geometry, exhumation history, and foreland sedimentation: Earth-Science Reviews, v. 76, n. 1–2, p. 1–131, http://dx.doi.org/10.1016/j.earscirev.2005.05.004